View metadata, citation and similar papers at core.ac.uk
brought to you by CORE
provided by NASA Technical Reports Server

N70-10774 T-46122

RESEARCH ON DIGITAL TRANSDUCER PRINCIPLES

Volume VIII

ELECTRICAL CONDUCTION MECHANISMS IN METAL-SEMICONDUCTOR-POLYMER THIN FILM STRUCTURES

CASE FILE COPY

ELECTRONIC MATERIALS RESEARCH LABORATORY

THE UNIVERSITY OF TEXAS

COLLEGE OF ENGINEERING

AUSTIN

RESEARCH ON DIGITAL TRANSDUCER PRINCIPLES

Volume VIII

ELECTRICAL CONDUCTION MECHANISMS IN METAL-SEMICONDUCTOR-POLYMER THIN FILM STRUCTURES

for the

NATIONAL AERONAUTICS AND SPACE ADMINISTRATION

Grant NGR-44-012-043

Covering the Period

July 1, 1967 - June 30, 1968

by

Lieh Chun Wang

William H. Hartwig

The University of Texas at Austin

Austin, Texas 78712

PREFACE

Previous work on Metal-Polymer-Silicon thin film structures by Wilmsen, Fitzgibbons, Wang, Chuang and Hartwig has been reported as part of the research on digital transducer concepts. The charge transport mechanisms of the polymer and behavior of the silicon surface and bulk were shown to be rather complex. The separate effort on polymer film properties, as reported in Volume VIII, shows behaviors which can be attributed to the dielectric alone. It is necessary to form the entire MPS structure to observe characteristics of the silicon surface. As a result, a separate project was undertaken to measure more carefully the combined behavior and then resolve the silicon surface (and bulk) effects.

Parallel work from the literature on MOS Field Effect Transistors was found to provide some clues as to the expected behavior, but it must be realized these devices have very thick insulating layers compared to those under study here. Since the charge transport is an exponential function of thickness (whatever the mechanisms), dielectrics which are only 100 Å thick would be expected to have a more critical role. This is deliberate, since eventual transducer behavior would draw, in some ways, upon the properties of the dielectric films. By making familiar capacitance vs voltage plots in addition to log current density vs square root of voltage plots, the effects of silicon surface states were to be resolved. From a knowledge of the voltage-current density behavior of the polymer alone, the field penetration into the silicon could be measured from reverse-biased data. From the differences, suitably corrected for work-function effects, would come the separate voltage drops across the polymer and silicon depletion layer. If successful, the increased knowledge would be useful in control of the break characteristics of the reverse-biased MPS structure.

ABSTRACT

Electron conduction mechanisms of metal-polymer-semiconductor systems were investigated in this project. Samples were made on N-type silicon of resistivity range 10Ω-cm to 150Ω-cm. A low energy electron (≈350 ev) gun was employed to polymerize the D.C. 704 pump oil used in the vacuum system. Metals of Al and Ag were evaporated on the polymer as top electrode.

Poole-Frenkel effects have been observed as the dominating conduction mechanism of the polymer. However, the I-V characteristics of MPS devices are different in the forward and reverse bias conditions. In forward direction, the current is dominated by the field within the polymer and increases exponentially with bias voltage in the fashion of Poole-Frenkel effect. In the reverse direction, three distinguishable regions may be obtained for the I-V characteristics on a ln J vs V plot. These were interpreted in terms of the proportion of voltage drops across the polymer and semiconductor to the total bias voltages. The generation of electron-hole pairs in the depletion layer of the semiconductor limits the current flow in the reverse bias condition and current saturation may be observed.

The I-V characteristics of MPS devices were found extremely sensitive to silicon surface preparation. Strong chemical etching was preferred for observing current saturations.

The experimental values of the slope of $\ln\sigma$ vs. $E^{1/2}/kT$ fell in the range of 6.55×10^{-23} to 8.7×10^{-23} and the zero field conductivity was 10^{-16} and 10^{-17} mhos/cm.

TABLE OF CONTENTS

	Page
PREFACE	iv
ABSTRACT	v
LIST OF FIGURES	viii
I. INTRODUCTION	1
A. Chemical Structure	1
B. Possible Conduction Mechanisms	3
1. Ionic Conduction	4
2. Space-charge-limited Flow	4
3. Tunneling or Field Emission	5
4. Schottky Emission	5
5. The Poole-Frenkel Effect	5
C. Limitation of The Theoretical Approach	5
II. THEORY	9
A. Conduction Processes through Thin Insulating Films	9
1. Schottky Emission	9
2. Tunneling	12
3. Poole-Frenkel Effect	15
B. Semiconductor Surface States and D-C Current Saturation	20
III. EXPERIMENTAL PROCEDURES	27
A. Sample Preparation	27
B. Back Side Contact	28
C. Polymer Formation	30
D. Electroplate Deposition	31
E. Sample Testing	32

Page

IV. EXPERIMENTAL RESULTS 34

A. Conduction Properties of Polymer 35

B. Data of MPS Devices 38

C. An explanation of I-V Characteristics of MPS Devices in Reverse Bias Condition 44

V. CONCLUSION 59

BIBLIOGRAPHY 61

VITA 64

LIST OF FIGURES

Number		Page
1	Energy-band Diagram of MIS Interface in Equilibrium	9
2	One-dimensional Tunneling	12
3	An Insulator Band Model. E_t and E_d are energy levels for Traps and Donors	16
4	Mechanism of Poole-Frenkel Effect	18
5	Potential Energy of an Electron within Periodic Crystal Lattice	21
6	Cathode Ray Tube Circuit	31
7	Testing Sample Connection	32
8	Current versus square root voltage of MPS device	37
9	I-V Characteristics of MPS Devices (Group 1)	39
10	I-V Characteristics of MPS Devices (Group 2)	40
11	I-V Characteristics of MPS Devices (Group 3)	41
12	I-V Characteristics of MPS Devices (Group 4)	42
13	Conductivity Versus Square-root of Electric Field	45
14	(a) I-V Characteristics of Sample #81	47
	(b) Current versus voltage drop across the semiconductor of Sample #81	47
15	Voltage drop across the polymer versus total applied voltage	49
16	Voltage drop across the semiconductor versus total bias voltage	49
17	Capacitance versus voltage of Sample #81	50
18	Energy diagram of the field-induced P-N Junction	56
19	Cross-section of an MPS Device	57

CHAPTER I

INTRODUCTION

This research project consists of two parts: the investigation of electrical conductivity of thin polymer films produced by electron bombardment of diffusion pump fluid silicone Dow Corning 704 and the surface state effect on D-C conduction mechanism of the Metal-polymer-semiconductor devices. The project serves as the first phase in developing a voltage/current digital transducer in thin film integrated circuit form by using the MPS devices as a basic transition element.

Before considering the theoretical and experimental work, the structure and likely polymerization products of the parent fluid (D.C. 704) must be considered.

A. Chemical Structure

The residual atmosphere in a kinetic vacuum system usually contains a mixture of gaseous compounds based on the elements carbon, hydrogen and oxygen. Thus typical gases and vapors present are water and oxides. Certain organic compounds such as methane are also present. They are emitted from vacuum pumps particularily those using organic fluids. It had been found[1] when mixtures of these gases were exposed to electrical discharges at low pressures a series of complex reactions involving decomposition, systhesis, oxidation and reduction could take place, and organic vapors were usually forming polymer condensation products. Thus, the breaking of chemical bonds, such as $-\overset{|}{\underset{|}{C}}-H$, $-\overset{|}{\underset{|}{C}}-\overset{|}{\underset{|}{C}}-$ and $= C = O$,

produces highly reactive groups which combine to form longer molecules. Hillier[2] and Watson[3] observed that the interaction of hydrocarbon vapor and electrons promoted polymerization and showed that the interaction occurred at the surface of the bombarded specimen in an electron microscope.

Holland and Laurenson[4] found that the chemical formula of silicone 704 with a uniform molecular weight of 485 must be of the following form, although the specific arrangement of methyl and phenyl groups are not known.

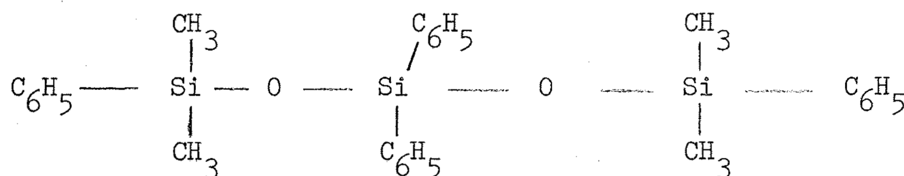

Exposure of silicone D.C. 704 to arc discharges and gamma radiation releases mainly hydrogen and methane with much smaller quantities of benzene. The resin remaining will therefore contain methylene and ethylene linkages between silicone atoms along with many of the original linkages. The methylene and ethylene bonds might be as follows:

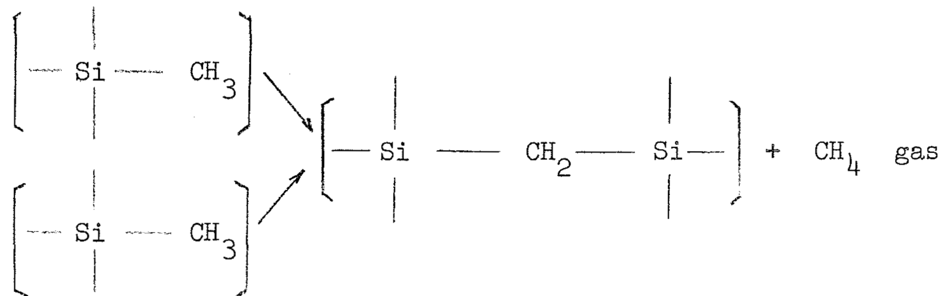

Methylene Cross Link

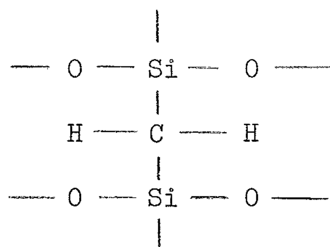

or

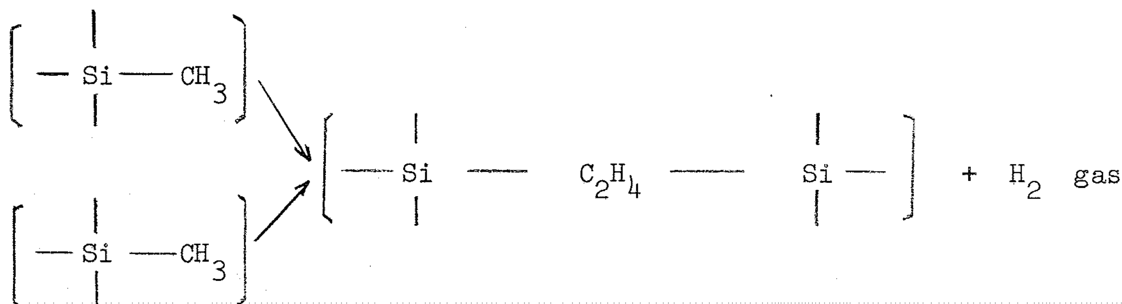

ethylene cross link

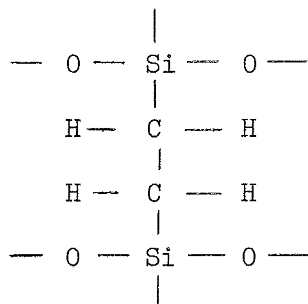

These linkages and cross links form a solid film with properties resembling those of silica.

B. Possible Conduction Mechanisms

At the outset, it has been assumed that the normal energy band concept can be applied directly to thin films of insulating materials. But thin films are frequently amorphous or polycrystalline and the band theory, applied to metals and semiconductors, is usually associated with the periodic

structure of the lattice. However, the energy spectrum of electrons in amorphous substances or liquids can be justified to have a band structure in "exactly" the same manner as a crystal so long as the short range order remains unchanged[5]. Thus the energy spectrum of an amorphous or even liquid semiconductor can be calculated just as in a crystal if the short range order is known.

By assuming that the normal energy band structure can be applied to an amorphous or polycrystalline material five possible conduction mechanisms through thin insulating films would appear.

The names and general characteristics of these five mechanisms are briefly described below and a more detailed analysis of some mechanisms is given in Chapter II.

1. Ionic conduction: It associates with the drift of defects in the bulk of insulators under the influence of an applied electric field. In amorphous films this mechanism may be important because a large number of defects exist. For films which absorb moisture from the atmosphere the bulk ionic conduction will also be enhanced.

2. Space-charge-limited flow: Carriers injected into the conduction band of the insulator continue to flow toward the anode due to the applied field. If no compensating charges are present, the carriers constitute a space charge, which in turn changes the field distribution in the insulator. There are several possible variants of space-charge limited flow depending on whether the current is due to electrons, electrons and holes, or whether traps or recombination centers are present. For an unlimited reservior of carriers in a trap-free insulator, currents up to 20 amps/cm^2

through the insulating (CdS) crystals had been observed. However, the presence of traps will reduce the current since any empty traps will remove most of injected carriers.

3. Tunneling or field emission: When the energy of an electron is less than the barrier height there is still a finite probability that the electron will "penetrate" or tunnel through the barrier. The current due to such an electron transition as tunneling is field emission from a thermionic cathode. The main problem in this mechanism is to calculate the transmission probability of an electron through a potential barrier by wave mechanics.

4. Schottky emission: This mechanism of current transfer is a high-field emission of hot electrons from a metal into the conduction band of an insulator in contact with it. It is a process identical with Schottky emission into the vacuum. The characteristics of Schottky emmision are its high temperature dependence and a plot of the logarithm of current versus the square root of bias voltage is a very good straight line.

5. The Poole-Frenkel effect: The Poole-Frenkel effect is the lowering of a Coulombic potential barrier when it interacts with an electric field, and is usually associated with the lowering of a trap barrier in the bulk of an insulator. An electron will be thermally excited into the conduction band by the amount the applied field energy lowers the potential barrier around a trap site. Frenkel had calculated the amount of lowering as twice the lowering of Schottky emission[6].

C. Limitations of The Theoretical Approach

The first limitation comes from the assumption that the thin

film insulators have a reasonably simple band structure as a crystalline material. This is not always true. Therefore, when applying the theories to amorphous and polycrystalline films, especially to the polymer, the exact chemical structure of which is not known, one can not expect a rigorous agreement between the experimental and theoretical results.

The second limitation is due to the presence of surface states at any metal-insulator or semiconductor-insulator interface. The unsaturated bonds and impurities at an interface will appear as localized energy levels in the forbidden band. These allowed energy levels are possible sources of charge and can thus have a strong influence on any conduction mechanism. Considerable experimental work has been carried out to study this problem in metal-SiO_2-Si films, but the results vary considerably. This is due to the pronounced sensitivity of surface states to the surface preparation, oxidation processes, and past history of the surface.. Results are not necessarily characteristic of oxidize surfaces in general but only of the specific treatments utilized.

Chang, Stiles, and Esaki[7] have studied the tunneling process between Al-Al_2O_3-SnTe and -GeTe junctions, where the semiconductor is degenerate P type. Their derived theory predicted a negative-resistance region in "forward"* direction. The negative resistance region happens

* The forward bias direction in this project refers to the condition where an accummlation layer forms at the semiconductor and insulator interface. That is, the condition when positive bias voltage is applied to the metal when the semiconductor is N-type or negative bias voltage is applied to the metal when the semiconductor is P-type. On the other hand, the reverse bias direction refers to the condition when a depletion layer forms in the interface, that is, positive bias is applied to metal P-type semiconductor or negative bias to metal for N-type semiconductor.

when bias voltage, V, is $F_p < qV < F_p + E_g$, where F_p is the Fermi level or degenerate P-type semiconductor and E_g is the band gap. At this condition the electrons in the metal in the energy range $qV - F_p$ cannot tunnel, since they are opposite the energy gap on the semiconductor side. Although the electrons within F_p are able to tunnel, the tunneling barrier is increased and as a result, the current should decrease with increasing voltage giving rise to a negative resistance. However, according to Chang,et.al the actual decrease of current in the negative-resistance region is always smaller than that predicted theoretically. In fact, in some samples, the current never decreases but merely shows a change of curvature. They believe that tunneling associated with gap states in the semiconductor is mainly responsible for the excess current as in a tunnel diode. Beside, the experimental excess current can not be correlated in any systematic manner with other known parameters of junction. The random nature also indicates the participation of interface states, since such states can hardly be controlled during fabrication.

Dahlke[8] found that the dc conductance of $Si-SiO_2-(Cr + Au)$ devices using P^{++} type Si and thin oxide layer ($< 50^{\circ}A$) showed one to two orders of magnitude increase by changing from annealed-steam grown, to steam grown and to dry-oxygen-grown oxide layers. This observation is explained by Dahlke as a corresponding increase of interface state density of oxide layers from annealed-steam grown to steam-grown and to dry-oxygen grown.

Wilmsen[9] investigated the "tunneling" between a metal and silicon

separated by a polymerized silicones film. His experimental MIS curves on both N and P type silicon show the exponential dependence of current on voltage and that the mechanisms for MIM and MIS tunneling are quite similar. An assymetric saturation of the MIS tunneling occurs when the device is reverse biased after certain voltage. This is caused by the formation of a depletion layer on the semiconductor which forms after completely charging the surface states. Based upon Wilmsen's model, the voltage/current transducer concept originates. This model will be further discussed in Chapter II.

Although the experimental results observed by some groups of experimenters did not agree completely with other group's experiments there was enough consistency to suggest three things:

1. The interface states definitely affect the electron transport mechanism in MIS systems.

2. The interface states must be controlled during the fabrication processes as well as possible.

3. The effects are random in nature, which may make the performances and parameters of these devices nonreproducible and unstable. They also indicate the development of methods of surface treatment for semiconductor devices are necessary.

CHAPTER II

THEORY

Theory of Metal-insulator-Semiconductor current mechanisms will be first discussed in this chapter, then the surface states effects and Wilmsen's model of current saturation will be described in detail.

A. Conduction Processes through Thin Insulating Films

As stated in Chapter I, conduction through insulating layers can take place by various mechanisms. However, tunneling, Schottky emission, and Poole-Frenkel effect have been observed in many thin polymer films[9,10,11,12], emphasis is given to these three mechanisms.

1. Schottky Emission

Consider the energy-band diagram of a Metal-Insulator-Semiconductor interface in Figure 1.

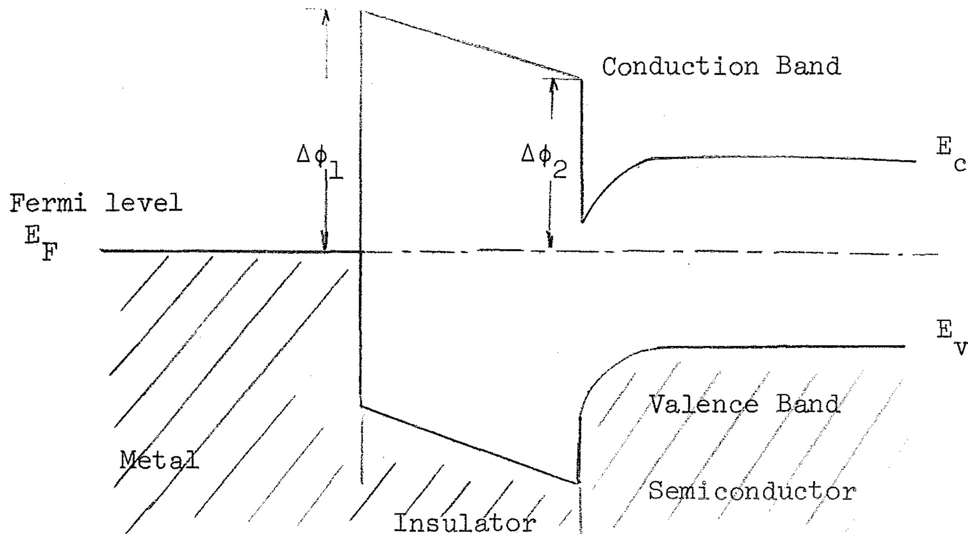

Fig. 1 Energy-band Diagram of a MIS Interface in Equilibrium

At high temperature, or when the energy barrier, $\Delta\phi$, is small, there will be electrons in the metal or semiconductor with sufficient energy to pass over the barrier and flow into the conduction band of the insulator. In equilibrium, an equal number of electrons flow in the opposite direction. By applying an electric field, the contribution of one group diminishes.

The current density can be calculated by integrating over all electrons in the metal or semiconductor with sufficient momentum to overcome the barrier. This closely resembles the Richardson equation in the case of thermionic emission into vacuum[13].

$$J = \left(\frac{4\pi m^* q k^2}{h^3}\right) T^2 \exp\left(-\frac{q\Delta\phi}{kT}\right) \qquad (1)$$

where m* is the electron effective mass in the insulator, T is temperature in ^{o}K, $\Delta\phi$ in ev, and h and k are Planck's and Boltzmann's constant respectively.

At normal temperatures, the thermionic current is negligible. However, the current will increase appreciably as high fields lower the barrier. This is analogous to the Schottky effect in thermionic emission from metal into a vacuum. The maximum barrier lowering can be calculated by the image force method as

$$\Delta\phi_{max} = \left\{\frac{qE}{4\pi\varepsilon_o K}\right\}^{1/2}$$

where E is the electric field in volts/cm, and $\varepsilon_o K$ is the permittivity of the insulator.

The effective barrier is then

$$\Delta\phi' = \Delta\phi - \Delta\phi_{max}$$

Inserting the effective barrier expression into the thermionic emission gives the Schottky equation

$$J = \frac{4\pi q m^* k^2 T^2}{h^3} \cdot \exp\left[-\frac{q\Delta\phi}{kT}\right] \cdot \exp\left[\frac{q \cdot (qE)^{1/2}}{2(\pi\varepsilon_o K)^{1/2} kT}\right]$$

$$= 120 \frac{m^*}{m} T^2 e^{-1.16 \times 10^4 \frac{\Delta\phi}{T}} e^{\frac{4.4}{T}\left[\frac{E}{K}\right]^{1/2}} \qquad (2)$$

where K is relative dielectric constant.

Equation (2) can be rewritten as

$$J = \alpha \exp(\beta E^{1/2}) \qquad (3)$$

$$\text{where } \alpha = 120 \frac{m^*}{m} T^2 e^{-1.16 \times 10^4 \frac{\Delta\phi}{T}}$$

$$\beta = \frac{4.4}{\sqrt{K}T}$$

The plot of Log J vs $E^{1/2}$ is a very good straight line, the intercept on the axis of Log J giving the value of α. This provides a way of estimating metal-insulator work functions, since by observing the value of α, the $\Delta\phi$ can be calculated directly.

2. Tunneling

Tunneling is a quantum mechanical process, which says there is a finite probability that a number of electrons without sufficient energy can "leak" through the potential barrier. Referring to the following figure and applying a WKB approximation[14] the probability P(E), that an electron incident on the barrier will pass through is

$$P(E) = \frac{|\psi_2(Z)|^2}{|\psi_1(Z)|^2} \approx \exp \left\{ - \int_{Z_1}^{Z_2} [2m^* [U'(Z) - E]^{1/2} dz \right\} \quad (4)$$

where $U'(Z)$ is the real barrier and E is the energy of the electron measured from the bottom of the conduction band of the metal.

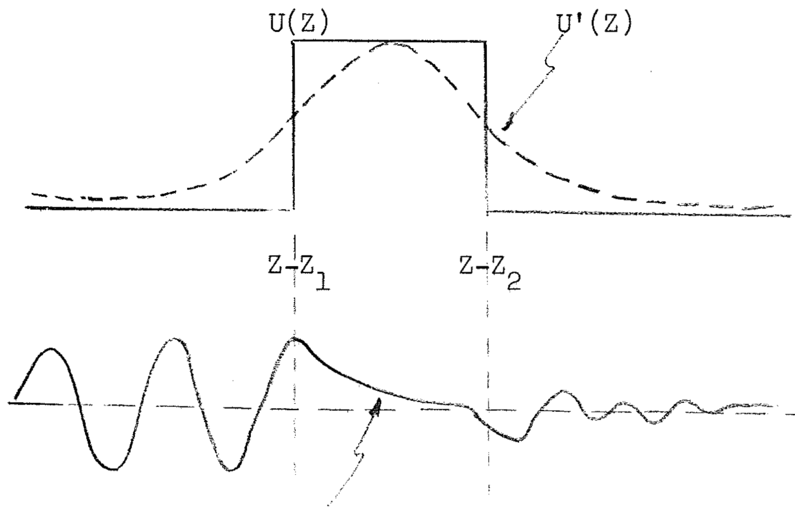

Fig. 2 One-dimensional Tunneling

From the above equation we know that the transmission probability is exponentially dependent on the thickness of the barrier or insulator.

For a very thin insulating layer (less than 50 Å) electrons may tunnel directly from a metal through the forbidden band into the conduction band of the other metal. For thicker insulator the tunneling probability is negligible, but an applied high electric field across the insulator can narrow the barrier and permit electrons to tunnel into the insulator conduction band. There are also tunneling processes which transport charge in and out of traps of the insulator.

The tunnel current passing through the insulator can be calculated by evaluating the integral

$$J_z = q \int N(E) \cdot f(E) \cdot V_z \cdot P(E) \cdot dKz \qquad (5)$$

where N(E) is the density of states function

f(E) is the Fermi function

Vz is the z component of velocity

Kz is the wave number of the electron and is expressed in the terms of energy.

There have been many attempts to evaluate the above equation, but the complete solution cannot be obtained in analytical form. Approximate calculations have been made by most authors, yet it may be valid only in certain limits. Two of the most recent and complete calculations are by Stratton[15] and Simmons[16]. For films of this study (>50 Å), direct tunneling from the conduction band of one electrode into another can be neglected. Tunneling from the conduction band of the

electrode into the conduction band of the insulator due to narrowing of the barrier by the electric-field, however, is possible. Simmons gives the expression for this condition as[19]

$$J = \frac{2.2q^3E^2}{8\pi h\,\phi} \exp\left\{-\frac{8\pi(2m)^{1/2}(\phi)^{3/2}}{2.96hqE}\right\} \qquad (6)$$

Although there are some inconsistencies which indicates an inadequacy of the idealized theoretical model (and the difficulities of the controlling the junction fabrication techniques), the main features of the theoretical analyses have been corroborated[7] .

Recently, tunneling studies have been extended to Metal-Insulator-Semiconductor junctions[7,17,18]. Chang, Stiles, and Esaki have given theoretical current-voltage expressions, in particular, for the case when the semiconductor is a degenerate p type. Wilmsen investigated tunneling between a metal and silicon separated by a thin insulating polymer and developed a model describing the current-voltage characteristics. The model shows that the electric field in the insulator controls the MIS current while the charge distribution in the silicon determines the insulator field. Wilmsen also indicated that the mechanisms for MIM and MIS tunneling are quite similar and an asymmetric saturation of the MIS tunneling was caused by the formation of a depletion layer on the semiconductor which formed after completely charging the surface states.

When surface effects are not considered, Wilmsen gave the

tunneling current expression as

$$Jx = Jo \frac{2\pi C_{10} kT}{Sin(\pi C_{10} kT)} \exp \left\{ -b_{12} (V_A - V_G)^2 \right\} Sinh \left\{ \frac{C_{10}}{2} (V_A - V_G) \right\} \quad (7)$$

Where b_{12} and C_{10} are smaller for MIS than for MIM, and V_G accounted empirically for the semiconductor energy gap. The constants b_{12} and C_{10} are functions of the physical parameters of the insulator, i.e., dielectric constant, thickness and effective mass. Of particular importance is the dependence of b_{12} and C_{10} upon L^{-2} and L^{-1} respectively, where L is the thickness of the insulator.

3. Poole Frenkel Effect

Real insulators have large quantities of imperfections. Each imperfection introduces one or more localized energy states which can be donor or acceptor type. High concentration of imperfections can change the conduction phenomena in thin-film insulators. States which are empty in equilibrium may trap free excess carriers, removing them from the conduction process. Localized imperfections also can scatter free charge carriers, thereby reducing their mobility.

By extending the model used to explain the conductivity of semiconductors, a model suitable for explaining the conductivity of insulators with traps can be obtained[20,21]. The energy band structure of one of these models is shown in Figure 3.

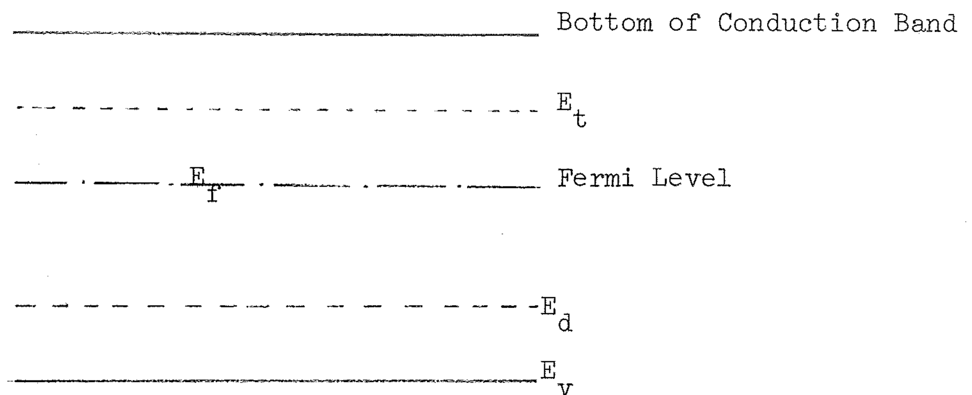

Fig. 3 In Insulator Band Model. E_t and E_d are energy levels for traps and donors

By equating the number of electrons missing from donor centers to the number of occupied traps and assuming the number of electrons in the conduction band can be neglected, the position of a "Fermi" level can be located. Let N_t and N_d be traps per cm^3 and donors per cm^3 respectively. Then,

$$N_d\, e^{-(E_d - E_F)/kT} = N_t\, e^{-(E_f - E_t)/kT}$$

from which,

$$E_F = 1/(E_d + E_t) + 1/2\ kT \ln N_t/N_d \tag{8}$$

At zero bias or low voltage the concentration of free electrons is due to the thermal energy of the insulator. The number of free electrons n,

is given by

$$n = N_c \ e^{-E_F/kT}$$

$$= N_c \ (N_d/Nt)^{1/2} \ e^{-(E_d + E_t)/2kT} \qquad (9)$$

where Nc is the effective density of states in the insulator.

Recall the expression for the conductivity of a material is

$$\sigma = nq\mu \quad \text{ohm-cm} \qquad (10)$$

Where n is the concentration of free carriers,

μ is the mobility of the carrier, and

q is the charge on the carrier

Therefore, the conductivity of the imperfect insulator a low field is[21,22]

$$\sigma_o = q\mu \ N_c(N_d/N_t)^{1/2} \ e^{-(E_d + E_t)/2kT} \qquad (11)$$

and the current density is

$$I_o = q\mu n \ V_b/L$$

$$= q\mu N_c \ (\frac{V_b}{L}) \ (N_d/N_t)^{1/2} \ e^{-(E_d + E_t)/2kT} \qquad (12)$$

where V_b is the bias voltage and

L is the thickness of the insulator.

At high fields, the field interacts with the trap barrier in the insulator and lowering it by an amount of

$$\Delta E = (q^3 \; Vb/\pi\varepsilon_o KL)^{1/2}$$

or

$$\Delta\phi = \left(\frac{qE}{\pi\varepsilon_o K}\right)^{1/2} = \beta_{PF} \qquad (13)$$

where $E = \frac{Vb}{L}$ is the applied field and

K is the relative dielectric constant.

Referring to figure 4, this field lowering of the barrier is known as the Poole-Frenkel effect. It results in the conductivity being field-dependent

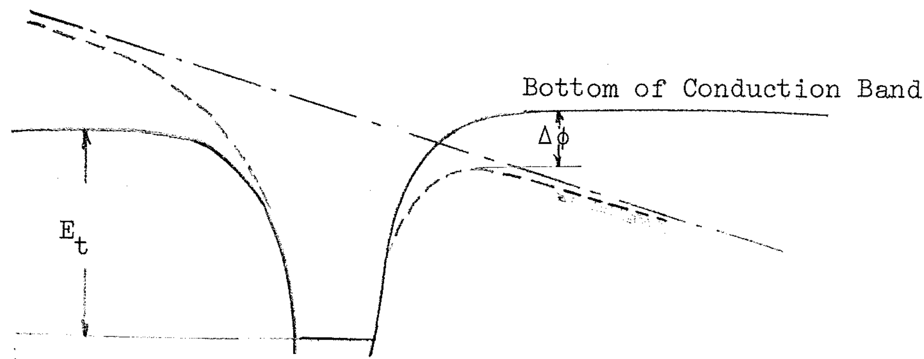

Fig 4. Mechanism of Poole-Frenkel Effect

since it drastically increases the carrier concentration. The number of free electrons in the conduction band increases to[21]

$$n = Nc \; (N_d/N_t)^{1/2} \exp\left\{-\frac{E_t + (E_d - \beta_{PF} E^{1/2})}{2kT}\right\} \qquad (14)$$

and the conductivity becomes

$$\sigma = \sigma_o \exp\,(\beta_{PF} E^{1/2}/2kT)$$

$$= \sigma_o \exp\,(\frac{\beta_{PF}}{2})\; E^{1/2}/kT) \qquad (15)$$

The general expression for Schottky emission, (equation (3) of this Chapter) can be rewritten as

$$J = \alpha \exp\,(\beta_s\, E^{1/2}/kT)$$

where

$$\beta_s = \beta/kT$$

or

$$\sigma = \alpha_o \exp(\beta_s E^{1/2}/kT) \qquad (16)$$

where

$$\alpha_o = \frac{\alpha L}{Vb}$$

Comparing equations (15) and (16) it can be seen that both the Schottky and Poole-Frenkel effects give the conductivity a field dependence of the same form.

The Poole-Frenkel conductivity, however, is of service only when the conduction process is bulk limited, and the Richardson-Schottky conductivity when it is electrode-limited. Therefore, if Poole-Frenkel emission

dominates, the current characteristics are insensitive to changes in polarity and the type of metal used as electrodes. If Schottky emission dominates, a large difference in current magnitude at equal but opposite fields results when metal with different work functions form the electrodes.

The theoretical values of β_s and β_{PF} can be calculated accurately provided that the high-frequency dielectric constant for the insulator is known. Thus, one can theoretically differentiate between the two types of conductivity from their different rates of change of conductivity with field strength. A plot of ln σ versus $E^{1/2}/kT$ results in a straight line of slope β_s or β_{PF}. This experimentally determined slope can be compared with the theoretically calculated β_s and β_{PF} to help determine which mechanism is the dominant one.

B. Semiconductor Surface States and D-C Current Saturation

The complete description of the V-I characteristic involves the interface between a non-crystalline polymer and the single crystal bulk silicon. The theory must include surface state effects which modify the bulk theories of conductivity and capacitance and take into account charge transport not usually treated in the MOS capacitor theory.

The electron behavior in a crystal can best be described in terms of wave mechanics. The differential equation, whose solutions are wave-like functions, is the Schroedinger equation. In a one dimensional crystal lattice the potential energy of an electron can be approximated by a periodic array of square wells - the Kronig-Penney model. Because of termination of the periodicity at the surface of an actual crystal,

Tamm proposed a modified Kronig-Penney model energy diagram as shown in Figure 5[23]. The Schrodinger equation for an electron moving in such potential is:

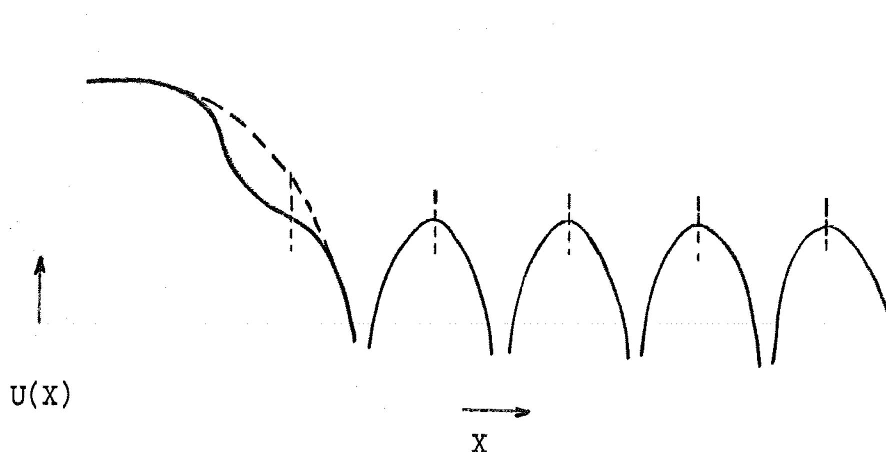

Figure 5 Potential Energy of An Electron within Periodic Crystal Lattice

a) Schematic representation of actual conditions.

b) Square-well approximation employed by Tamm.

$$\frac{d^2\psi}{dx^2} + \frac{2m}{\hbar^2} E\psi = 0 \qquad 0 < x < a;$$

$$\frac{d^2\psi}{dx^2} + \frac{2m}{\hbar^2} (E-V_o)\,\psi = 0, \qquad a < x < a + b; \tag{17}$$

$$\frac{d^2\psi}{dx^2} + \frac{2m}{\hbar^2} (E - W)\,\psi = 0 , \quad x < 0,$$

Where m and E are the mass and energy of an electron. The solutions of Schrodinger's equation are of the form

$$\psi(x) = U_k(x)\, e^{jkx}$$

where $U_k(x)$ is either a periodic function with the periodicity of the potential or a constant. The probability of finding an electron in any unit cell of the crystal has to be equal but the probability of finding an electron in a surface state should decrease as x increases. This leads to the argument that real values of k corresponding to energy states in the allowed energy bands and complex values of k corresponding to states in the forbidden band. Tamm was the first to realize that the localized states at the surface may be described with wavefunctions having complex values of k, since these types of states decrease exponentially from surface to bulk. These localized states are called Tamm states and are introduced as the asymmetrical termination of the periodic potential at the surface.

Contrasted with this, Shockley considered a symmetrical termination as shown in the dashed line of Figure 5. With this model Shockley showed that the surface states can only exist when the actual lattice constant is smaller than a certain minimum value. These are so-called Shockley surface states.

In addition to the Tamm or Shockley states, the impurities or defects in a real material will also introduce energy states in the forbidden band. For instance, phosphorus doped N-type silicon will introduce energy levels about 0.044 ev below the conduction band edge and on the other hand Boron will introduce levels about 0.048 ev

above the valence band edge[24]. In many cases, the semiconductor surface is covered with a layer of foreign material, such as an oxide, as either an accidental or deliberate result of the preparation procedure. States lying within or on the outer surface of such a layer are also commonly called surface states, even though they do not originate in the semiconductor itself[25]. There is no general mathematic solution for $\psi(x)$ which can be used on the MPS structure. It is recognized, however, all these classes of states may act as traps, recombination centers, or both, and thus may make the semiconductor surface "metallic" or change many properties of semiconducting devices. A phenomenologic theory is all that can be offered at this time.

The changing of DC conduction mechanisms of MIS devices due to interface state density is of special interest to this experiment and study, since it is the principle of the MPS digital transducer. Wilmsen proposed current saturation of the MPS device in reverse biased condition due to exhaustion of surface state changes. Wilmsen[9] stated that the silicon surface states cause an N-shift in the surface energy. The surface states are filled up to the Fermi level. When negative voltage is applied to the metal field plate, mobile electrons are removed from the surface states. This continues until the supply of electrons from the surface states is exhausted. When negative bias voltage is further increased a surface accumulation or depletion region will be formed depending upon the type of semiconductor. When positive voltage is applied to the metal field plate, mobile electrons are "driven" into the

surface states and this will continue until all the surface states are filled up. Again a surface accumulation or depletion region will be formed when the bias voltage is further increased. The important point is that the electric field was assumed to be entirely within the insulator until the surface states are exhausted. Recent experimental evidence has led to a relaxation of this requirement.

In a reverse-biased depletion region, for reverse bias $V_r >> kT/q$, the concentration of carriers is reduced well below their equilibrium concentration. The rate of generation of electron-hole pairs in such a situation can be obtained from the equations for electron-hole pair recombination-generation in the bulk of semiconductor[30,31] by letting $p, n << n_i$. This leads to

$$U = - \frac{\sigma_p \sigma_n U_{th} N_t N_i}{\left[\sigma_n e^{(E_t - E_i)/kT}\right] \left[\sigma_p e^{(E_i - E_t)/kT}\right]} = \frac{Ni}{2\tau_o} \qquad (18)$$

where T_o is the effective lifetime within a reverse-biased depletion region and is given by

$$T_o = \frac{\sigma_n e^{(E_t - E_i)/kT} + \sigma_p e^{(E_i - E_t)/kT}}{2\sigma_p \sigma_n V_{th} N_t}$$

σ_p, σ_n = capture cross-section of holes and electrons

V_{th} = thermal velocity of carriers

N_t = concentration of bulk recombination-generation centers per unit volume

E_t = energy level of recombination-generation center

E_i = electron energy at the intrinsic Fermi Level.

The generation current, which is extremely important in analysis the I-V characteristics of MPS devices in reverse bias condition is proportional to the generation rate U. Another factor which affects the generation current is the depletion layer width. For a P-N junction this width is expressed as

$$W = \left[\frac{2K_s \varepsilon_o}{q} \; \frac{N_a + N_d}{N_a N_d} \; \phi_T \right]^{1/2} \quad (19)$$

where ϕ_T is referred to as the built-in voltage ϕ_b of a p-n junction

In the MIS capacitor structure, if a small reverse bias voltage is applied, a depletion region tends to form. The charge per unit area contained in this depletion region is $Q_s = - qN_d W$ (assume N-type Si). If the reverse bias voltage is further increased, a very narrow inversion layer may start to form. In an equilibrium case, that is no D-C current flow through the capacitor, the width of the depletion layer reaches a maximum. Thus, under strong inversion conditions the charge per unit area induced the semiconductor will be given as

$$Q_s = Q_{in} - qN_d W_{max}$$

where Q_{in} is charge in the inversion layer. An important point is that a small increase in depletion region width may result in a very large increase in the charge contained within the inversion layer.

In the MPS devices, current can flow through the polymer, therefore, a non-equilibrium situation exists when the device is reverse biased.

The depletion layer width may never reach a maximum value, but would increase very slowly when bias voltage is continuously increased.

Wilmsen observed the current saturation of MPS capacitors in the reverse biased condition and explained it as field penetration into the semiconductor when surface states have been exhausted. Therefore, the surface states act like a "transition switch"; before it's exhausted it shields the semiconductor surface and makes the semiconductor behave like a "metal". The current passing through the MPS device will be increasing exponentially with bias voltage just like current conducting in MPM devices. After the surface states have been exhausted, the "metal" behaves like semiconductor again. Thereafter electric field lines terminate on the charges in the depletion region. It is now apparent this explanation can be modified by inclusion of Q_{in} in the model. The impact of such a model on the realization of a digital device behavior would be very beneficial since it would provide a rational means to relate physical behavior at the "break" to parameters which may be controlled.

CHAPTER III

EXPERIMENTAL PROCEDURES

A. Sample Preparation

Previous research on MIM or MOS junctions showed that the device performance and yields were extremely sensitive to surface preparation and smoothness. For this reason two categories of silicon wafers were used in the experiment.

1. Commerically available mechanically polished medium resistivity both P and N type silicon wafer (∿ 10 ohm-cm, from Texas Instruments).

2. Mechanically lapped and chemically polished N type silicon wafers prepared in the Electronic Materials Research Laboratory of The University of Texas (∿ 30 ohm-cm to ∿ 250 ohm-cm). The lapping and polishing process for group two wafers are:

a) The wafer preparation begins with a single crystal silicon boule cut into 25 mil slices with a diamond wheel.

b) The 25 mil slice is lapped with # 240 alumina grit to remove the saw damage. The #240 grit is removed by rinsing in deionized water and by ultra-sonically cleaning in methyl alcohol.

c) Step B is repeated with #400, #600 and 5 micron grits to obtain a scratch-free surface prior to chemical polishing.

d) The ultra-sonically clean wafer is etched with CP-4 about 70 seconds. During this etching process the wafer should be agitated all the time in the breaker. The etching is stopped by quickly adding deionized water to the CP-4 A smooth mirror surface should be achieved.

Both groups of the wafers should have the identical and strict cleaning procedures as follows:

a) Clean all glassware and other hardware to be used in the cleaning process with non-ionic detergent and glass cleaning solution,

b) Scrub the silicon wafer with the non-ionic detergent,

c) Rinse off the detergent with deionized water,

d) place the wafer in a 50 ml beaker and cover with fresh, dry methyl alcohol,

e) Ultra-sonically agitate for 30 seconds,

f) Pour off the methyl alcohol and cover with trichloroethylene,

g) Boil in the trichloroethylene for one minute,

h) Pour off the trichloroethylene and repeat step g,

i) Pour off the trichloroethylene and flush with deionized water five times,

j) Place the wafer in hydrofluoric acid for 30 seconds,

k) Flush with deionized water seven times,

l) cover the wafer with methyl alcohol,

m) steam the wafer with boiling trichloroethylene for 30 seconds and transfer to the vacuum chamber as quickly as possible.

B. Back Side Contact

Since high resistivity silicon (10 ohm-cm to 250 ohm-cm) is used in making the MPS device, this will inevitably introduce problems of preventing rectifying contacts. Three techniques have been adopted to insure good ohmic contacts:

a) silver deposition: Ohmic contact can be made to P-type material when the effective work function of the semiconductor is less than the work function of metal. For 10 ohm-cm p type silicon the effective work function is 4.2 ev and for silver the work function is 4.73 ev. Therefore, ohmic contact can be insured when the silver is evaporated on the p type silicon wafer. This silver deposition is usually made before polymerization takes place.

b) Electroless Nickel Plating: In electroless plating an electron interchange has to take place between two chemical species. The electroless nickel plating involves the catalytic reduction of nickel ions by sodium hypophosphite. The hypophosphite ion gives up electrons and becomes phosphite ion, and the nickel ion receives the electrons and deposits as metallic nickel. A typical bath for use on germanium or silicon may be made as follows:[27]

	grams/liter
Nickel chloride ($NiCl_2 \cdot 6H_2O$).	30
Sodium hypophosphite ($NaH_2PO_2 \cdot H_2O$).	10
Ammonium citrate [$(NH_4)_2HC_6H_5O_7$].	65
Ammonium chloride (NH_4Cl)	50
Filter	

Add ammonium hydroxide (NH_4OH) until the solution turns from green to blue. This is particularly useful on silicon, because soft-solder connection can be made to it at temperature below 200°C. For 10 ohm-cm N-type silicon, one electroless plating is sufficient for making ohmic contact. For higher resistivity material, improvement is made by alloying the nickel into the silicon at temperatures of 800 to 900°C. In the

latter case a second nickel plate is necessary. When this technique is used, the wafers are usually electroless plated before the cleaning process.

c) An Indium Gallium paste or a Mercury-Indium-Lead paste smeared onto the back side of silicon wafer offers another way of making ohmic contacts. Cleaness of the wafer is the essential factor for success of this method. Therefore, the paste is applied to the wafer immediately after the cleaning process.

C. Polymer Formation

The formation method and characteristics of the insulating thin polymer have been described by Ennos and Christy[28,29]. The polymerization process begins when low energy (≈350 ev) electrons break the bonds between radicals of an organic molecule. In this experiment, the Dow Corning 704 diffusion pump oil used in the vacuum systems served as a source of the organic molecules. An RCA 902 A cathode-ray-tube with the face portion of the tube removed is used as the supply of electrons for the polymerization. The schematic diagram for the cathode ray tube circuit is shown in figure 10.

A three station set-up and a rotary sample holder as described by Wilmsen[9] are installed in the bell jar of the vacuum system. The sample holder will first rotate the sample to the station, where the electron beam of the CRT will hit the film of oil molecules on the surface sample and the polymerization process will take place. The growth rate of the polymer is a function of the density of the electron beam, the pressure in the vacuum system, and the duration of time which the system has been

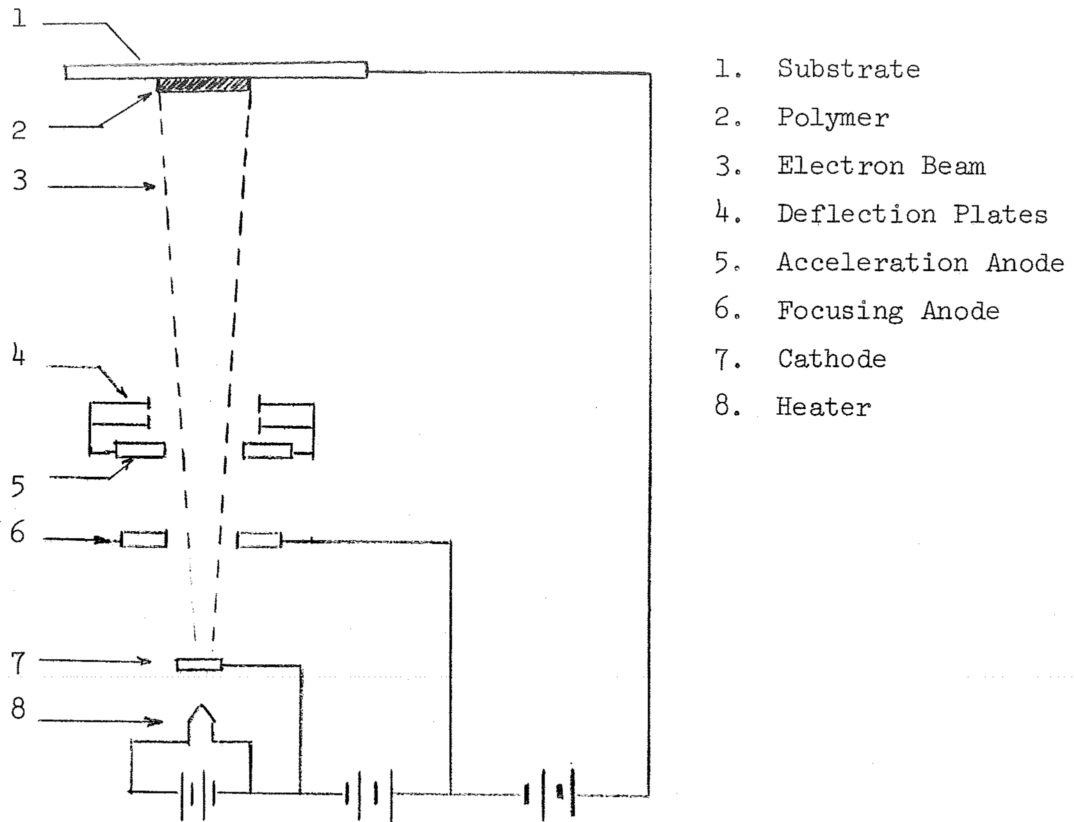

Fig. 6 Cathode Ray Tube Circuit

pumped down. For one and a half hours pump-down (the vacuum system reaches 5×10^{-5} torr and a beam current density of 4 micro-Amp/cm^2, the growth rate is about 1.8 Å/minute. By the polymerization station is a small crucible 1.5 cm in diameter fulled with D.C. 704 oil. When heated up to 60°C for one hour before polymerization, this crucible would supply an extra source of pump oil for polymerization and increase the growth rate to 2.8 Å/min.

D. Electroplate Deposition

After the polymer been formed on the silicon substrate, the sample was rotated to the first metal deposition position, where three aluminum

dots of 2.24 mm^2 each were vapor deposited on the polymer through a stainless steel mask. The filment current was maintained at 40 amps for 55 seconds. The polymer might be damaged by the heat radiated from the tungsten filment (Mathis No. F4-3-030a, three strands, 5 coil tungsten filment) for aluminum evaporation. A brass circular dish of 9 cm in diameter and 5 mm in thickness and with a concentric hole of 1.5 cm in diameter was held between the heating filment and the sample to serve as a heat shield.

After the aluminum dots had been deposited, the sample was allowed to stand about 10 minutes for the metal to anneal and order itself, then rotated to station three for silver evaporation. The process for silver deposition is similar to the aluminum, except the area of the silver dots is smaller (.85 mm^2) and the heat shielding brass disk is not used. Ten minutes of annealing and ordering time is again allowed before the sample is taken out of the vacuum for testing purpose.

E. Sample Testing

After construction the MPS device is completely enclosed in a special sample holder described by Yeargan[20] to avoid the surrounding electromagnetic field disturbances during measurements. The schemetic diagram for the holder is shown as following:

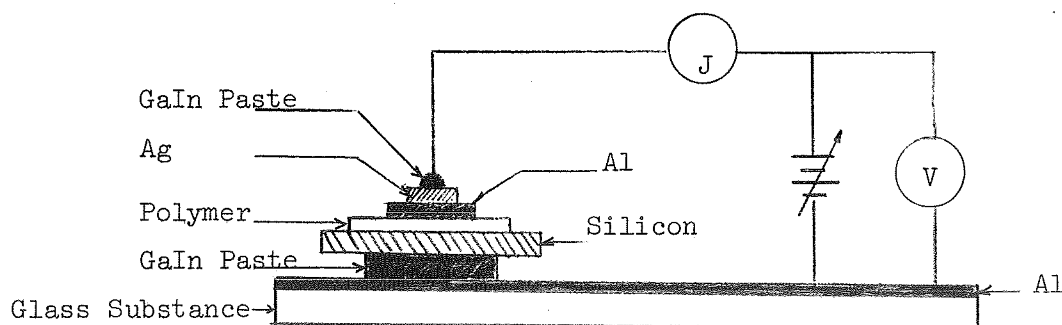

Fig. 7 Testing Sample Connection

The capacitance measurements of the device were made on a General Radio 1615 A capacitance bridge at 1 Kc. The thickness of the polymer were obtained through the relation,

$$d = \frac{K\varepsilon_o A}{C} \quad \text{(neglecting fringing)}$$

where K = relative dielectric constant,

A = the area of the aluminum filed plate,

C = the capacitance of the MPS device.

A Hewlett-Packard 425 A micromicro-ammeter and a Hewlett-Packard 413 A dc voltmeter measure the current and voltage respectively.

CHAPTER IV

EXPERIMENTAL RESULTS

For a period of ten months, more than eighty samples have been made for this research project. In the early stage, Ag-polymer-Si devices were made. Silver electrodes were used because the Ga-In eutectic "blob" wets it so well during measuring process, good electrical contact is always ensured. However, a large fraction of samples were shorted out. A group of samples made with tin, lead and nickel top electrodes were also shorted. Aluminum electrodes can always give positive results, but the Ga-In does not tend to wet the aluminum and good electrical contact is extremely difficult.

Therefore, an additional fabrication process is necessary to ensure good electrical contact and prevent short circuits. A new evaporation mask was cut and silver dots, smaller in diameter than the aluminum dots, were laid over the aluminum electrodes. With this configuration, aluminum was contiguous to the polymer and assured a high sample yield while silver was exposed in order to make good contact with the GaIn blob.

In the second period of the experiment successful samples, with reproduceable I-V characteristic, capacitance reading, and low dissipation factor, were continuously made in the laboratory. The thickness of polymer determined by capacitance measurement had been checked with ellipsometer measurement, it showed less than 10% of disagreement. Low dissipation factor (in the range of 0.001 to 0.04 at 1 KC) indicates good ohmic contact to the silicon wafers had been made. Most samples

were made on mechanically polished N-type 10Ω-cm silicon, a few were made on P-type or of higher resistivity (70-113Ω-cm) wafers. The thickness of polymer for those samples were around 150 Å.

No distinguishing saturation was observed for either polarity however. Two samples made on 80Ω cm N-type silicon showed the tendencies of saturation but the current never leveled off. From these results, two conclusions have been drawn:

1. Chemically polished silicon wafers may have to be used, since the mechanically prepared surface might have much higher surface state density simply because of mechanical damage of the surface during the lapping and polishing processes.

2. Thinner polymer is preferred, because it will decrease the saturation voltage.

Samples were made with chemically polished silicon wafers. A higher fraction of samples showed the saturation characteristics demonstrating a cause-and-effect relation had been established between surface preparation and onset of saturation for reverse biased MPS devices.

In the following sections the charge transport mechanisms in polymer and curves demonstrating current saturation, are discussed.

A. Conduction Properties of Polymer

The charge transport mechanisms in thin film polymers may best be observed and understood by making MPM capacitors. The reason is in MPS devices, the field penetration into the semiconductor and the existance of surface states in the polymer-semiconductor interface complicate the

problems.

Figure 8 shows a typical behavior of the current with bias of an MPM capacitor. The ln J vs $V^{1/2}$ is a very straight line, with a changing slope at higher bias. The straight line characteristic indicates that it is Schottky emission or Poole-Frenkel effect. The changing of slope suggests more than one mechanism may be involved. Theoretically, one can differentiate quite readily between Schottky emission and the Poole-Frenkel effect from their different rates of change of conductivity with field strength, that is a plot of kT lnσ versus $E^{1/2}$ results in a straight line of slope β_{PF} β_s, where $\beta_{PF} = 2\beta_s = \left[\frac{q^3}{\pi K \varepsilon_o}\right]^{1/2}$. Dielectric constant values from 2-4 were measured[4] depending on the formation conditions of the polymer. By taking K = 2.8 for the polymer[9,11] the theoretical values of β_{PF} and β_s were calculated to be 7.26×10^{-23} and 3.63×10^{-23} respectively. Simmons[21] says the high-frequency dielectric constant of the insulator should be used. By taking $K = n^2$, where n is the index of refraction of the polymer, then $K \simeq 2.0$, since the index of refraction measured for the polymer by ellipsometer is 1.39. For K = 2.0, the theoretical values for β_{PF} and β_s are 8.6×10^{-23} and 4.8×10^{-23} respectively. The experimentally determined β for sample #20 shown in Figure 8 is 6.55×10^{-23} for small slope segments and 8.7×10^{-23} for sharper slope segments. The conclusion is that the dominant conduction mechanism of the polymer is probably the bulk-limited Poole-Frenkel effect, since the experimentally determined β is closer to the theoretically calculated β_{PF}. More experimental evidence of a dominant Poole-Frenkel effect is shown in next section. The interceptions of the straight lines in

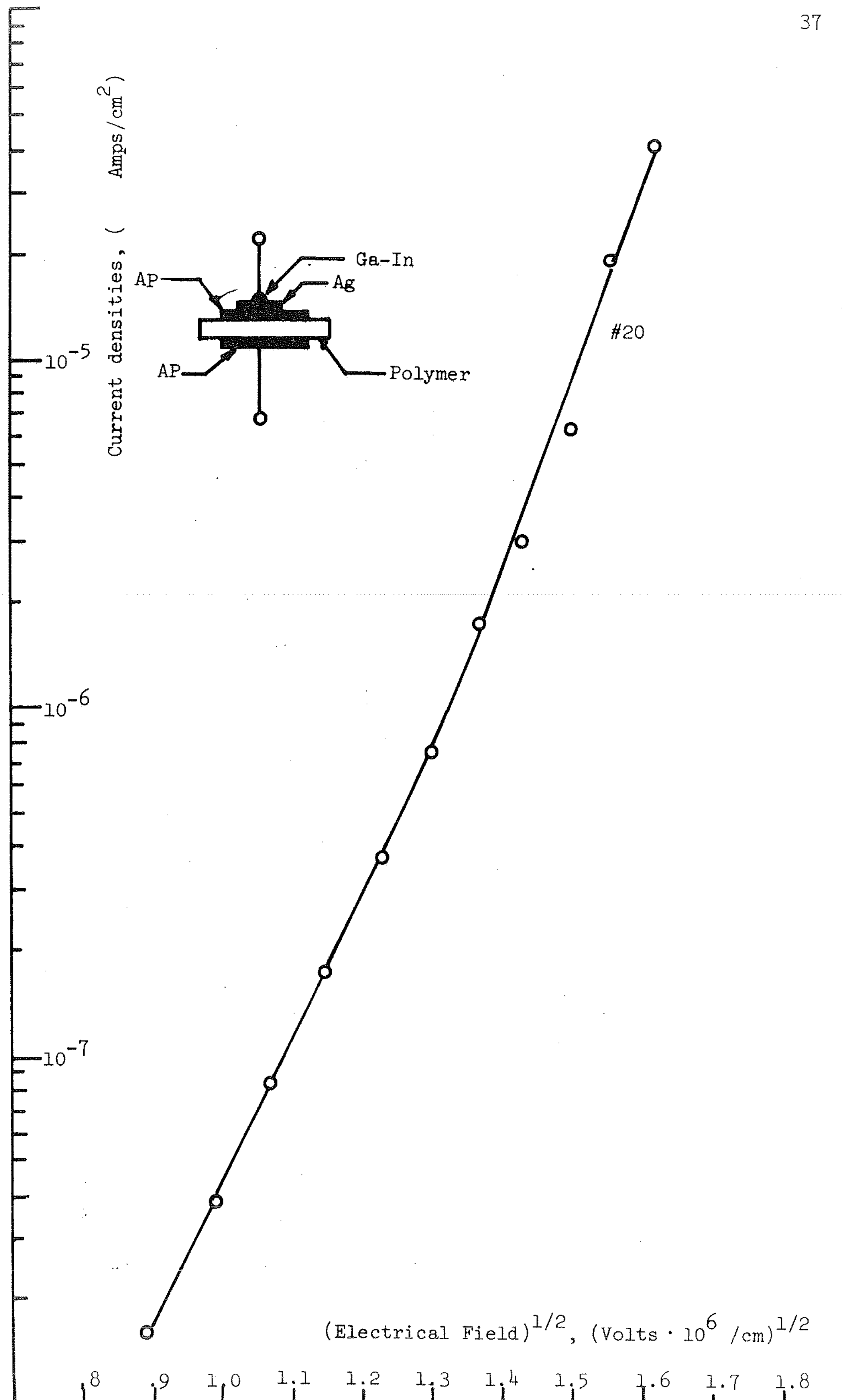

Fig. 8 Current versus Square-Root Voltage of MPS Devices

Figure 8 give $\sigma_o = 6.4 \times 10^{-16}$ and $\sigma_o = 5.8 \times 10^{-17}$ from Eq. 15.

A parallel study on charge transport in thin polymer films by Chuang[32] shows bulk-limited behavior accounts best for dissipation in the MPM capacitor. The Poole-Frenkel model is generally supported in these results. Previous tunneling models applied to MPS conduction required an arbitrary fit to theories of Simmons[19] and Stratton[15]. It is believed the evidence for dominant Poole-Frenkel effect is now more persuasive and will be adopted.

B. Data of MPS Devices

Four groups of current vs bias data of MPS devices are plotted in Figure 9 through 12. Those curves were plotted with currents versus voltages in order to bring most information of I-V characteristics of the MPS devices.

Figure 9 shows the I-V characteristics of two MPS devices with mechanically polished silicon wafers. It can be seen that the low resistivity (10 Ω-cm), and thicker films (140 Å) gives a symmetric I-V curves in the forward and reverse biased conditions. However, the curves of the device with higher resistivity (70 Ω-cm) and thinner film (80 Å) show an asymmetric characteristics. The slope of the I-V curves in reverse bias gradually decreases, which indicates the field begins penetrating into the semiconductor.

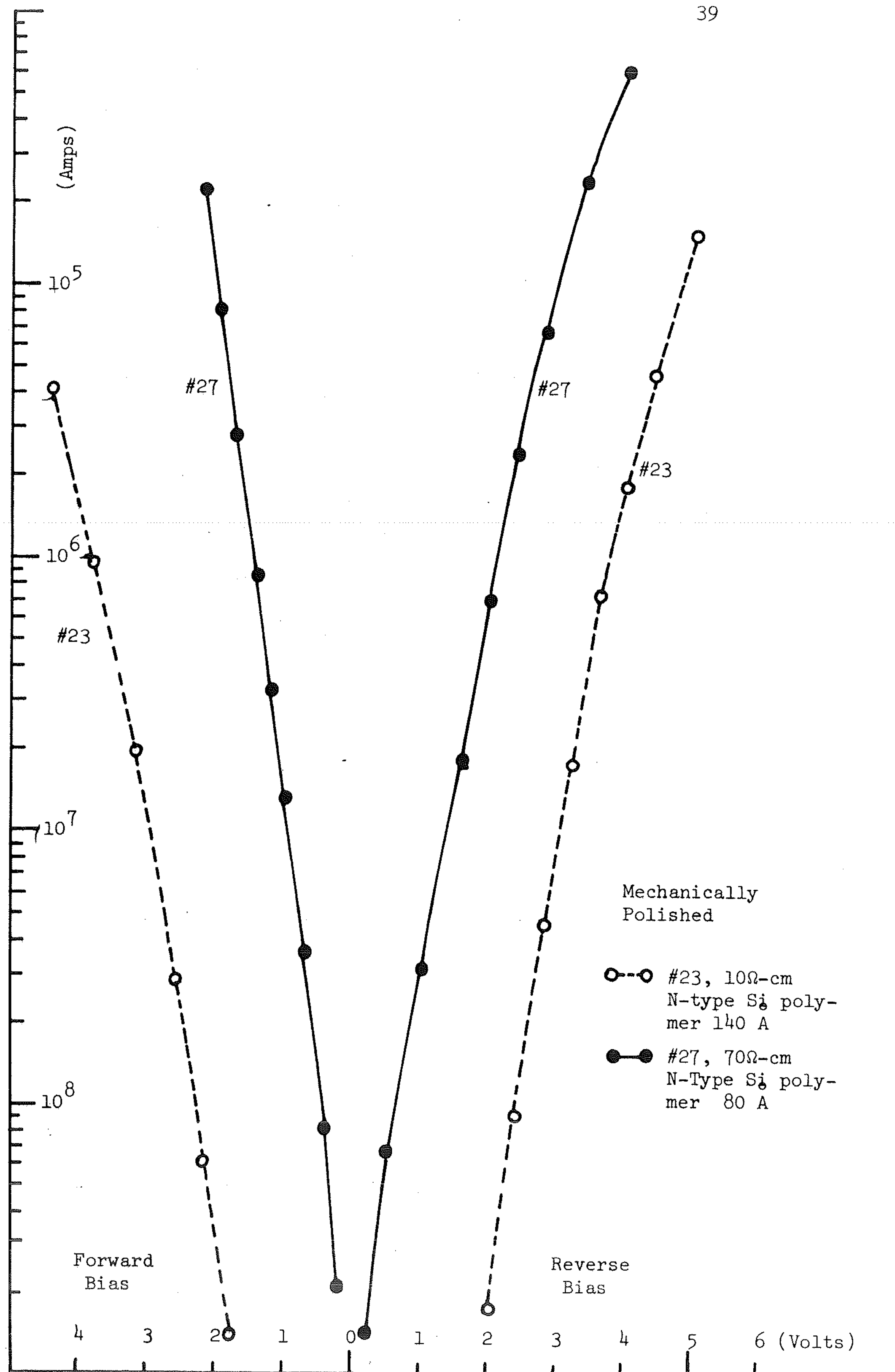

Fig. 9 I-V Characteristics of MPS Devices (Group 1)

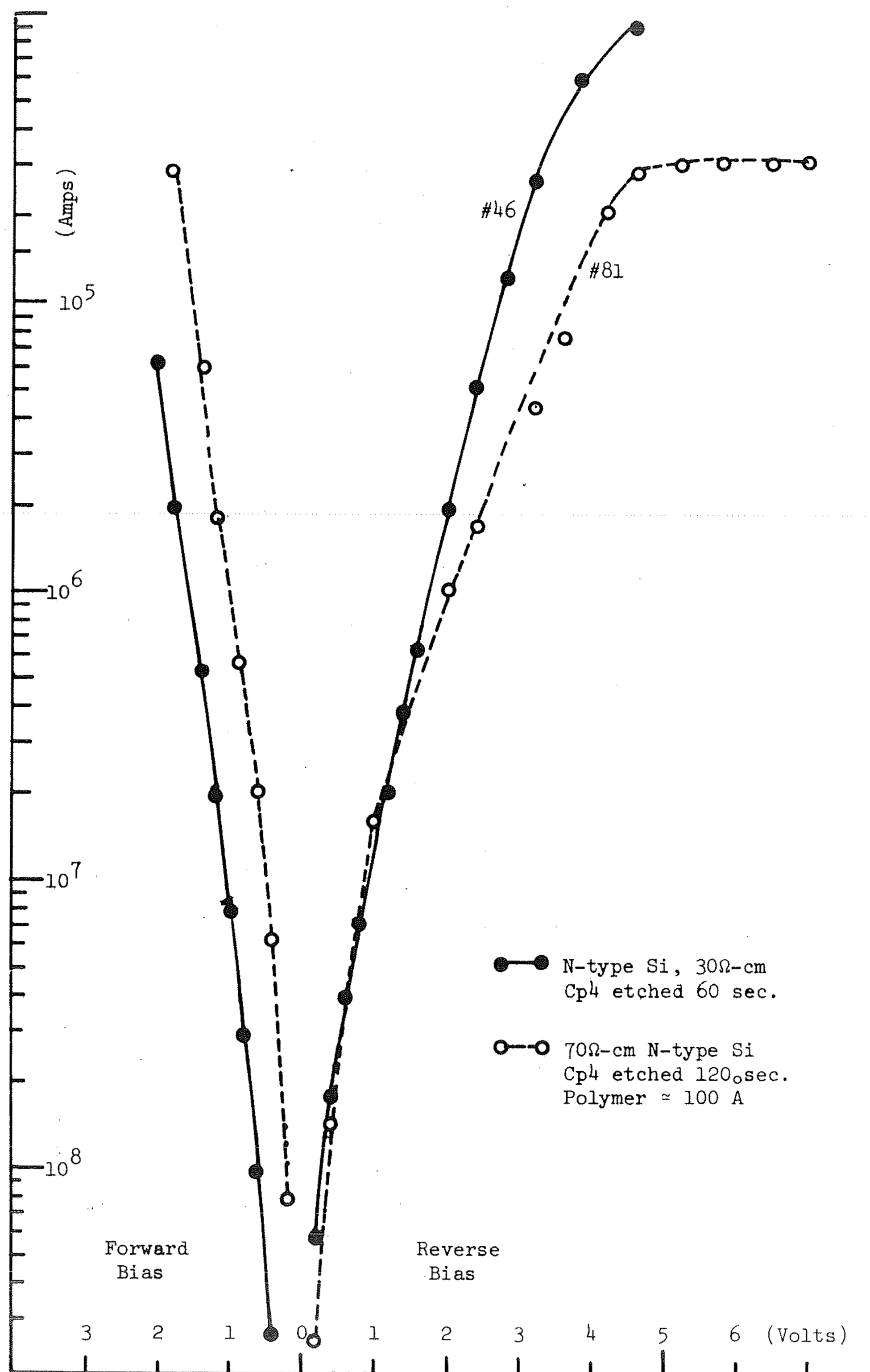

Fig. 10 I-V Characteristics of MPS Devices (Group 2)

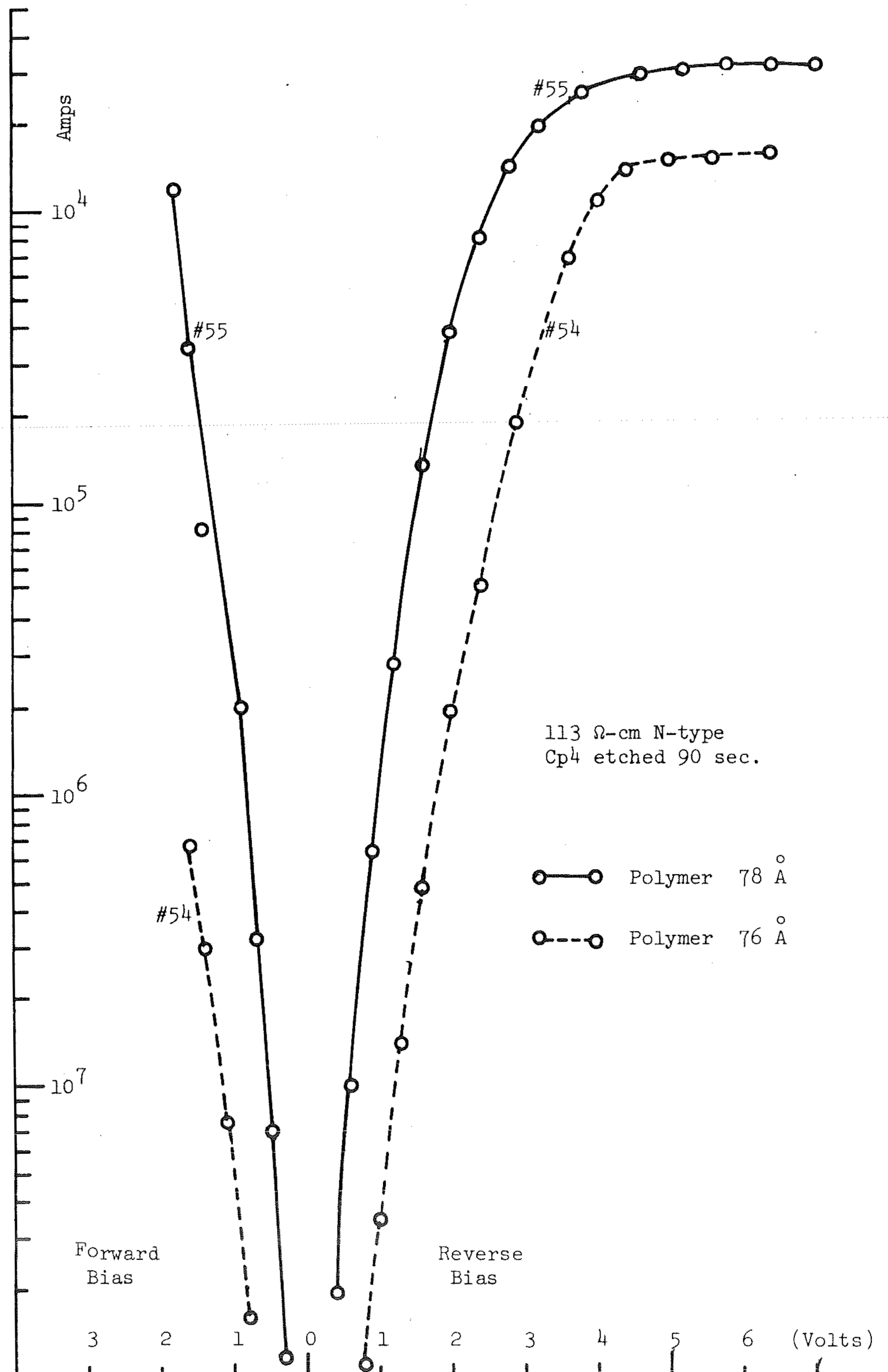

Fig. 11 I-V Characteristics of MPS Devices (Group 3)

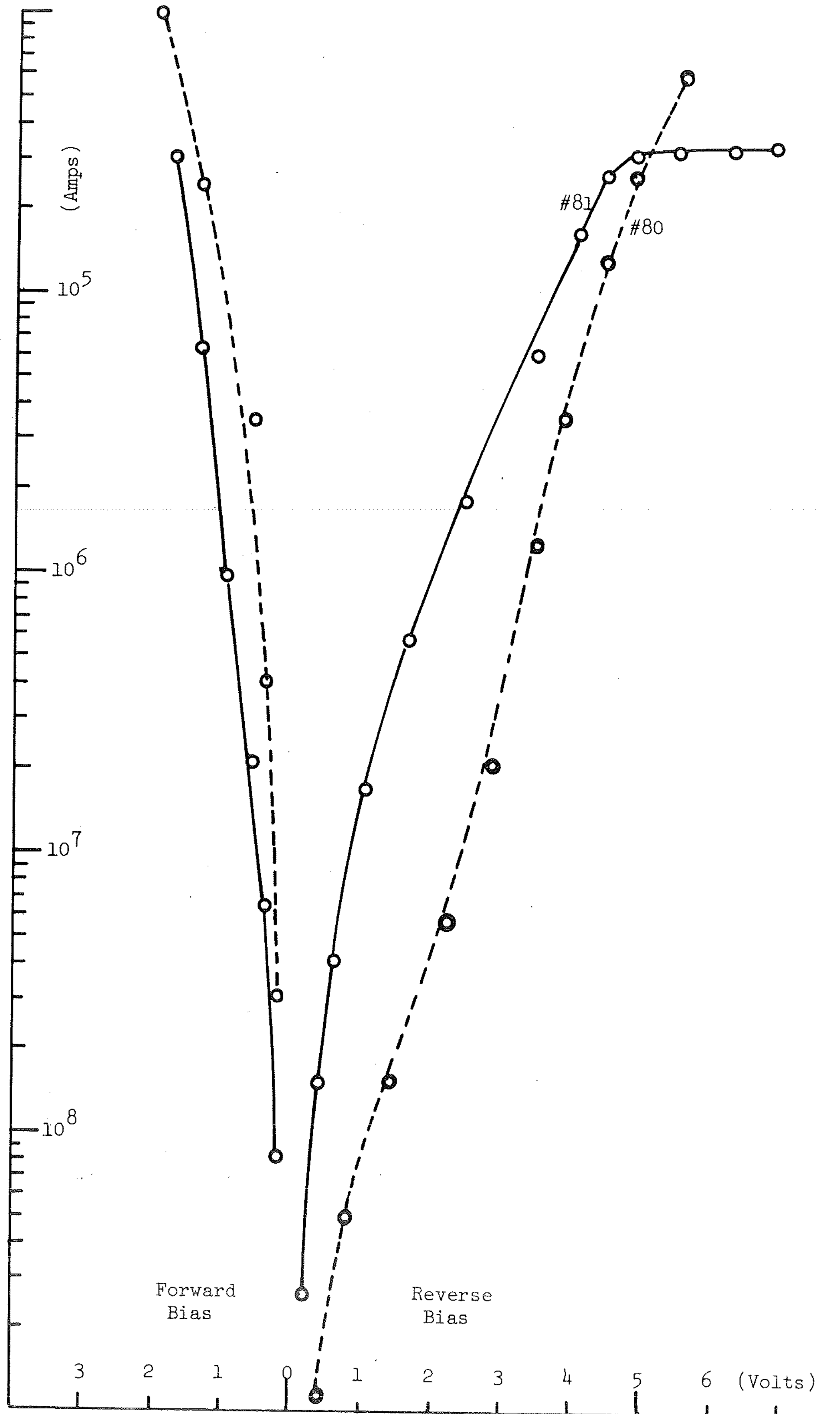

Fig. 12 I-V Characteristics of MPS Device (Group 4)

The I-V curves of two devices with chemically treated (etched with cp4) wafers were showed in figure 10. The I-V curves are asymmetric and a saturation was observed for the device with wafer of higher resistivity (70Ω-cm) and longer etching (120 sec). Figure 11 shows I-V curves of two adjacent devices (1 mm apart) made on the same wafer. The general shapes of the I-V plots are alike, however, the magnitude of currents varies one to two orders.

The I-V curves of another pair of devices, made on the same wafer are shown in Figure 12. The magnitude of currents of the two devices were different. One shows the saturation and the other does not.

From these data several conclusions can be drawn:

1. In forward bias condition: the I-V characteristic of the MPS devices are always similar. They are independent of the surface treatment and the resistivity of the silicon wafers being used. Furthermore, the lnI vs $V^{1/2}$ always yields straight lines. It is believed that the conduction mechanisms governing the MPM devices also govern the MPS devices in the forward bias condition.

2. In the reverse bias condition: The I-V curves vary from sample to sample. The curvatures are always in the direction of increasing dynamic resistance. It is extremely sensitive to surface treatment of the silicon wafers.

3. The formation of depletion layers and inversion layers in the semiconductor surface cause a field-penetration-limited conduction process. This is discussed in detail in the next section.

4. There is more than an 0.06 ev difference of work function between Al and Si (the work function of Al is 4.1 ev and N-type (10Ω-cm) Si is 3.8 ev). If the dominant mechanism is Schottky emission this should yield several orders of magnitude of current difference when changing the polarity of bias voltage on the MPS device. However, every device made, the reverse bias and forward bias currents show less than one order of magnitude of difference, especially before the inversion layer takes place. This is an evidence of a dominant Poole-Frenkel effect.

5. The current saturation in reverse bias voltage direction can only be seen in devices made on chemically polished and higher resistivity silicon wafers. However, this is a necessary but apparently not sufficient condition.

6. Field penetration into the semiconductor can be observed more easily in devices having thinner polymer films. For devices having thicker films, this penetration may possibly be observed at higher voltage or current levels.

C. An Explanation of I-V Characteristic of MPS Devices in Reverse Bias Condition

Sample #81 was selected for studying the I-V characteristics of MPS device in reverse-bias condition. The voltage drops across the semiconductor and the total bias voltage are separated from the data of forward and reverse current as plotted in Figure 14. This separation can only be justified if the work function difference between polymer and semiconductor is not significant enough to affect the magnitude of currents when changing the polarity of bias voltages. In other words, the mechanism

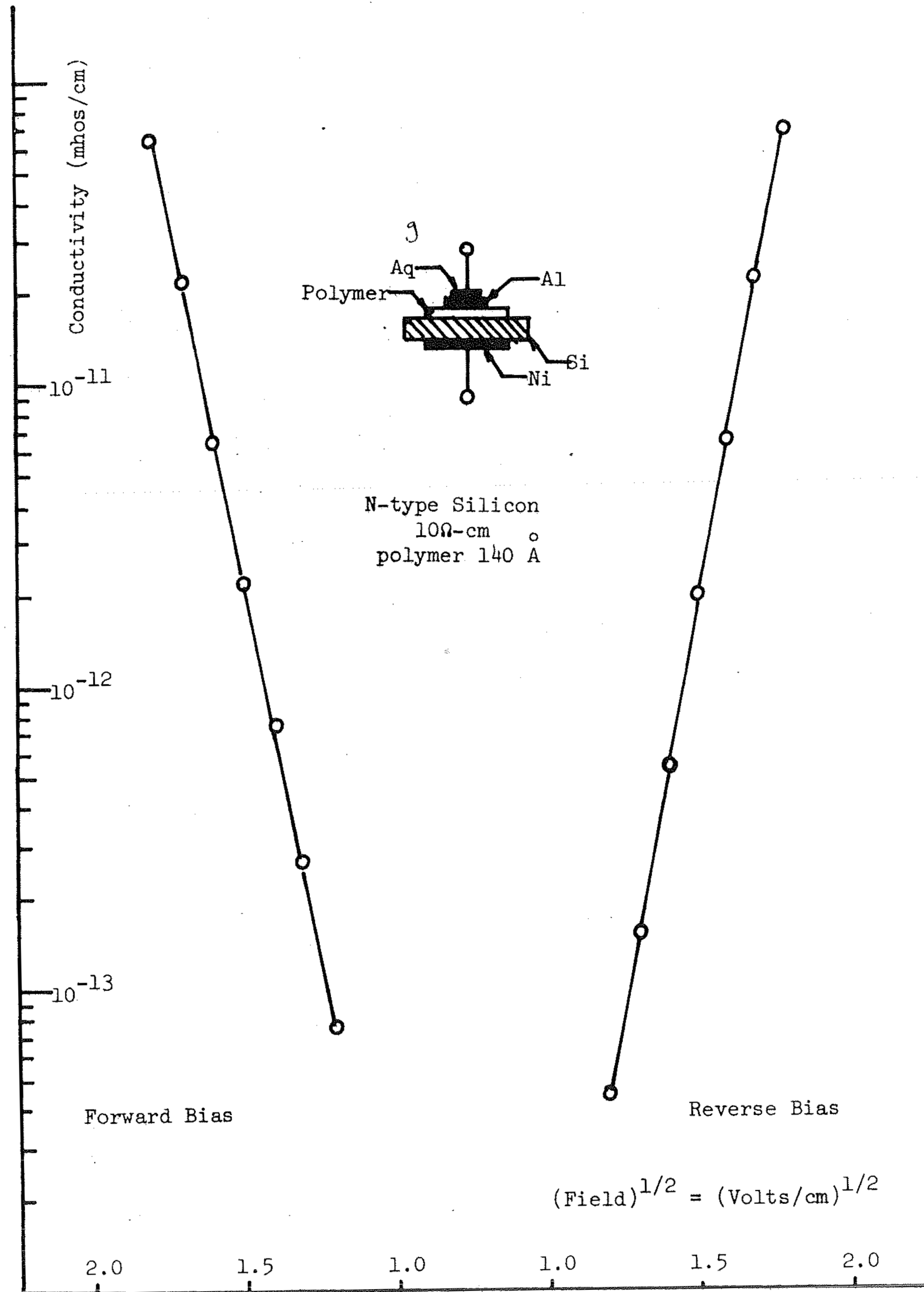

Fig. 13 Conductivity vs. Square-Root of Electric Field

of charge transported through the polymer has to be bulk-limited and independent of electrodes. Otherwise, the existence of contact potential may cause a rectification at the polymer-semiconductor interface. This rectifier could certainly distort the information for studying the I-V characteristics of the MPS devices in the reverse bias condition.

By examining the I-V-Characteristics of sample #23 in Figure 13 the justification is obtained. Sample #23 was made on a 10Ω cm N-type silicon and the polymer is much thicker (140 Å) than most other MPS devices (≈80 Å).

The conductivity *versus* square-root of field in the forward and reverse biased condition is plotted in figure 13, it can be seen that the plot is two straight lines and nearly symmetric with respect to zero bias. The work functions for Al and Silicon (10Ω cm, N-type) are 4.1 ev and 3.8 ev respectively. If it is an electrode limited conduction process, the conductances should vary by several orders of magnitude when changing the polarity of bias. This symmetry is strong evidence that the conduction mechanism is bulk-limited and justifies the assumption that no work function difference is being seen.

Two "impedances" corresponding to the voltage drop across the polymer and semiconductor can be associated with the MPS devices. However, both the impedances are non-linear. The impedance of the polymer is decreasing rapidly with bias voltage, and on the other hand, the impedance of the semiconductor will increase with increasing reverse bias. At low bias, essentially all the applied voltage appears across the polymer. When the applied voltage increases, the drop across the semi-

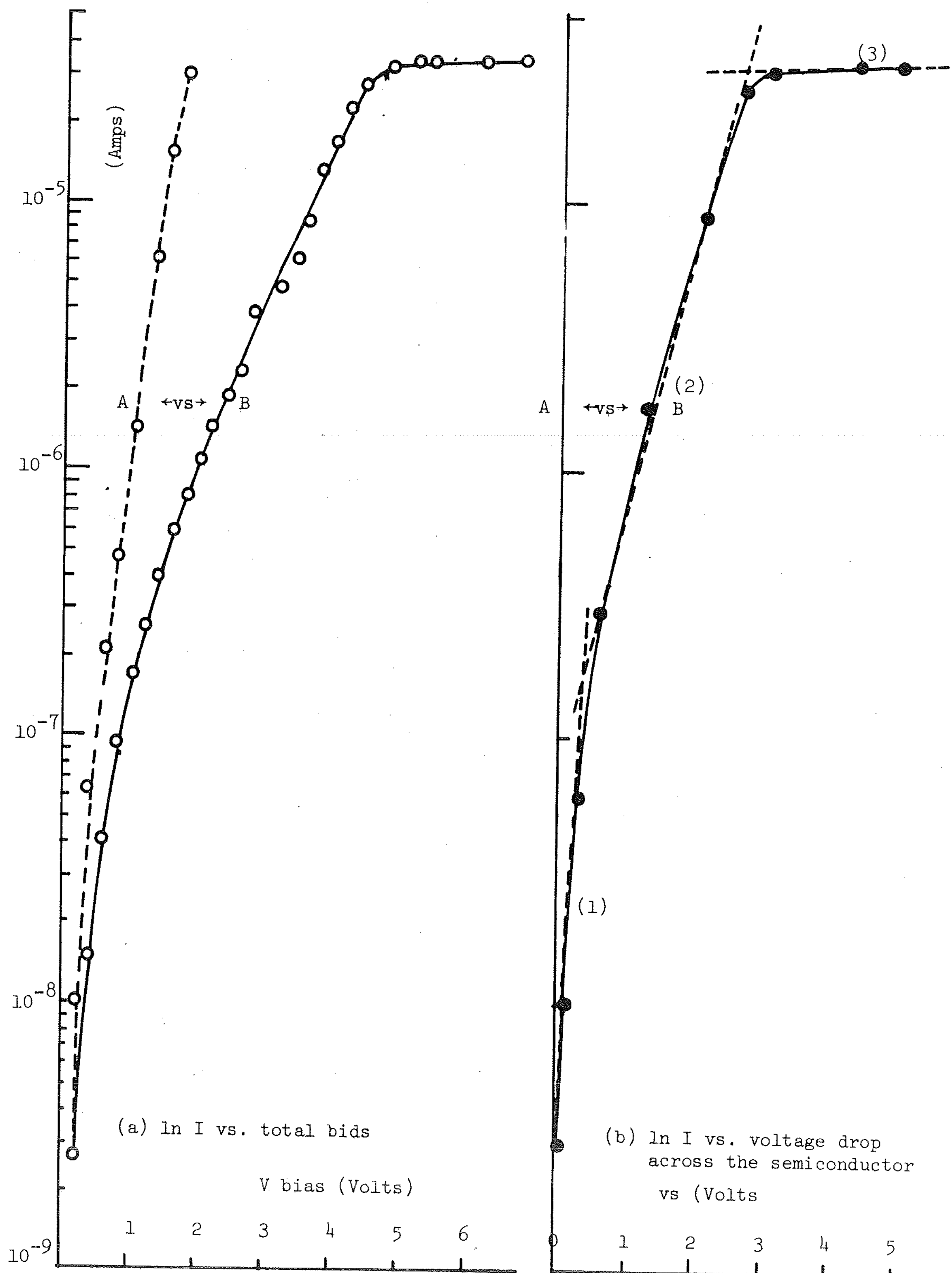

Fig. 14

conductor begins to appear, since the reverse biased semiconductor will begin to form a depletion region. At some transition voltage, the impedance of the semiconductor increases to a value equal to that of polymer. When this occurs, the applied voltage is shared equally between the polymer and semiconductor. Thereafter, more of the voltage in excess of this transition will fall across the semiconductor. The remaining fraction across the polymer is just sufficient to insure current continuity throughout the system.

For MPS devices of thicker polymer the transition voltage is expected to be much higher than the thinner one. Sample #32 shows the symmetric I-V curves within the bias voltage range of interest ($\leq$ 7Volts) and the thinner ones already show the onset of asymmetric characteristics. Bearing these in mind, we can construct a set of figures showing the current-voltage relation in the semiconductor. The voltage drop in the polymer and the voltage drop across the semiconductor are plotted versus the total applied voltage in Figure 15 and 16. With these curves in hand, plus the curve of capacitance versus bias voltage, a further analysis of the I-V characteristics of MPS devices in the reverse bias condition can be carried out.

Wilmsen stated that the current through a MPS device in reverse bias should saturate when the depletion layer in the semiconductor surface begins to form. This means current saturation happens at or before the complete formation of the depletion layer. By refering to figure 11 and 12 we see it is not true in our case, since the current saturated at a bias of about 4.8 volts and the depletion layer was completely formed around 1.2 volts.

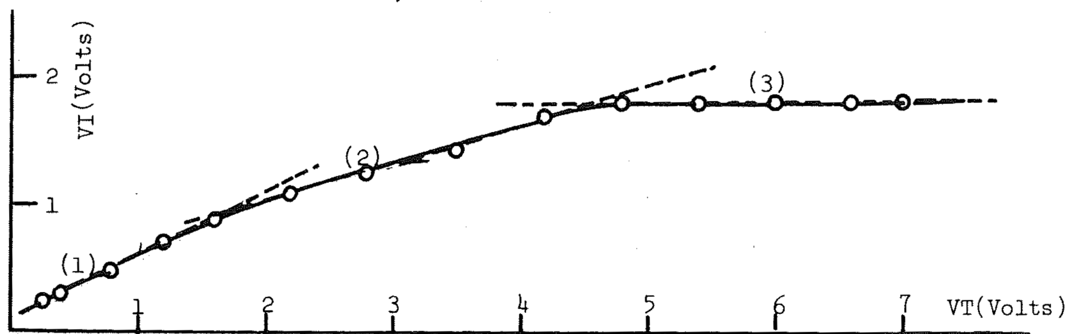

Fig. 15. Voltage drop across the polymer vs. Total applied voltage

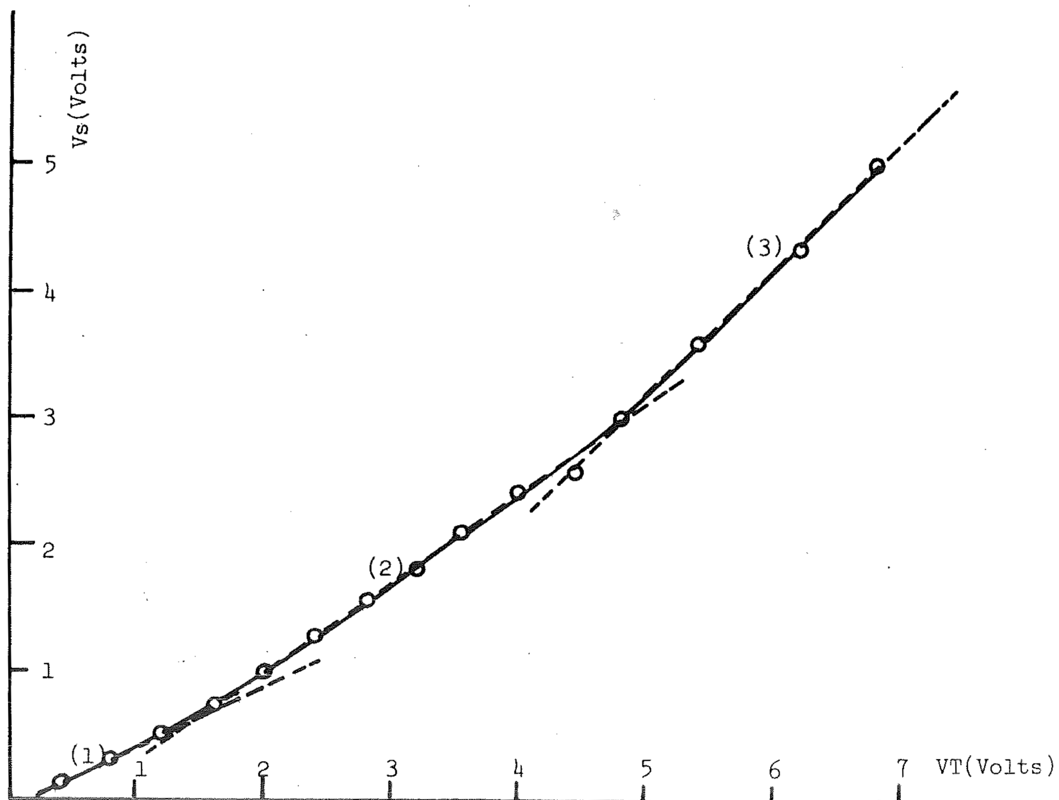

Fig. 16. Voltage drop across the semiconductor vs. total bias voltage

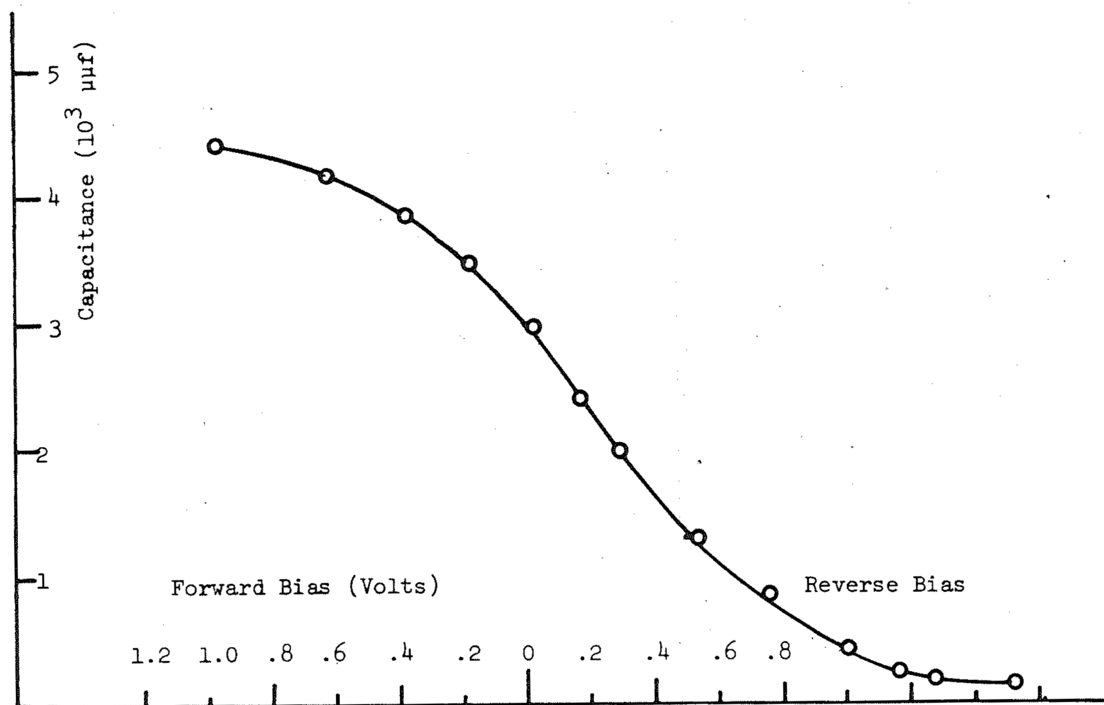

Fig. 17 Capacitance versus Voltage

Other mechanisms have to be adopted in order to explain the observed phenomena. As has been mentioned the total applied voltage or voltage drop across the MPS devices can be separated as voltage drops across the polymer and/or the semiconductor. By carefully studying figure 14, it can be seen that the voltage drop across the semiconductor may be divided into three regions if three approximation lines are drawn, by using the same piece-wise linear technique. Three distinguishable regions of different I-V characteristics can also be obtained in Figure 14b. The relationships between a region of one curve to the corresponding region in another curve will be stated clearly later on.

As figure 16 shows, in region (1) the total bias voltage begins to drop across the semiconductor. The formation of a depletion layer in the semiconductor causes the voltage drop. However, the voltage drop in the polymer (as shown in figure 15) is large as compared with that across the semiconductor, therefore, the current is dominated by the field across the polymer. The current increases sharply with bias voltage as shown in figure 14b and the injected electrons from the polymer to the depletion region will be quickly swept to the semiconductor electrode through the depletion layer.

In region (2), the voltage drop across the semiconductor is comparable with the voltage drop across the polymer. Due to the higher voltage drop an inversion layer apparently has begun to form at the semiconductor surface. This is substantiated by the capacitance vs bias voltage curve in figure 17, the formation of inversion layer causing the capacitance to approach a minimum value. Actually, then, there is

a field-induced p-n junction at the semiconductor surface. The voltage across the polymer is still increasing when the bias voltage increases. The rate of increase is slower, however, as can be seen in figure 15 where the slope of the curve gradually decreases. The result is still a polymer field dependent I-V curve, but the slope is gradually decreasing toward zero.

Since there is a field-induced p-n junction at the semiconductor surface, the injected electrons from the polymer may be combined with the ionic holes in the inversion layer. The inversion layer is not yet strongly inverted, therefore, the recombination rate is not high and it can be said that the mean free path of the injected electrons in this layer is longer than the width of the inversion layer. Injected electrons may recombine with holes in this region, but a large number will pass through to the neutral N region.

In region (3), the voltage drop across the semiconductor is continually increasing, its increasing rate is linearly proportional to the increase of bias voltage as can be seen in Figure 16. At this region, the inversion layer is strongly inverted, and the charge in this layer is tremendously increased. The result is that the current passing through the MPS device is completely limited by the recombination rate in the inversion layer. Since d-c current flow has to be maintained in the MPS system, holes from the depletion region have to be supplied to the inversion layer and an equal number of electrons in the depletion layer also have to move to the neutral N-type region. Thus, the current is equally well limited by the recombination-generation processes that take place in the field-induced junction.

Recall that in an ordinary reverse biased p-n junction there are two basic current components; the generation current in the depletion region of the junction and the diffusion current caused by electron-hole pair generation in the neutral P and N regions. In the neutral region there is no significant electric field present and the minority carriers move only by diffusion.

For the diffusion-current component, only those minority carriers which are generated within a diffusion length of the edge of the depletion region will contribute to the diffusion current, because only those have a chance to reach the edge of the depletion region. Thus one would expect the diffusion current to be given as

$$I_{diff} = q[\text{net generation rate per unit volume in the neutral region}] \times [\text{diffusion length}]. Aj$$

where Aj = junction cross-sectional area.

Assuming no illumination and $p_n << p_{no}$ or $n_p << n_{po}$, where p_n, n_p are concentration of holes or electron in an n-type or p-type semiconductor, and p_{no}, n_{po} are values of p_n, n_p in equilibrium, the diffusion current in the N-region can be given as

$$I_{diff,p} = q \frac{p_{no}}{\tau_p} L_p Aj$$

where τ_p is lifetime of holes in an N-type region, L_p is diffusion length. A similar expression can be given for I_{diff} in p region.

In a reverse-biased depletion region, the rate of generation of electron-hole pairs can be obtained as[30]

$$U = - \frac{n_i}{2\tau_o}$$

where τ_o is defined as the effective lifetime within a reverse-biased depletion region and is given by

$$\tau_o = \frac{\sigma_n e^{(E_t - E_i)/kT} + \sigma_p e^{(E_i - E_t)/kT}}{2\sigma_p \sigma_n V_{th} N_t}$$

where σ_n, σ_p = capture cross-section area of electron and the hole respectively

E_t = energy level of recombination

E_i = an electron energy at the intrinsic Fermi Level

V_{th} = thermal velocity of carriers

N_t = concentration of bulk recombination-generation centers per unit volume.

One electron-hole pair generated provides one electronic charge to the external circuit. Thus, the magnitude of current due to generation within the depletion region will be given by

$$I_{gen} = q|U| WAj = 1/2 \; q \frac{n_i}{\tau_o} WAj$$

The important point is that the generation-current component is dependent on the magnitude of the applied reverse bias. At higher bias W is larger, more centers are included within the depletion region, and the generation current increases in proportion to W.

In a reverse-biased P-N junction (assume a step junction), the total depletion region width W as a function of the total electrostatic, potential variation from one side of the junction to the other (ϕ_τ), is

$$W = \left\{ \frac{2K_s \varepsilon_o}{q} \quad \frac{N_a + N_d}{N_a N_d} \quad \phi_\tau \right\}^{1/2}$$

where ϕ_τ is referred to as the built-in voltage of a p-n junction and N_a and N_d are concentrations of acceptor and donor impurities.

A particular case of step junctions which is often encountered in practice is a step junction where one side is more heavily doped than the other, for example, $N_a \ll N_d$. This results in a simpler form for the depletion layer width,

$$W = \left\{ \frac{2K_s \varepsilon_o}{qN_d} \quad \phi_\tau \right\}^{1/2}$$

In our non-equilibrium field-induced p-n junction the above equation still holds, however, the ϕ_τ term has to be replaced by $\phi_b + \phi_s + V_a$, where ϕ_b, ϕ_s and V_a are defined in Figure 18.

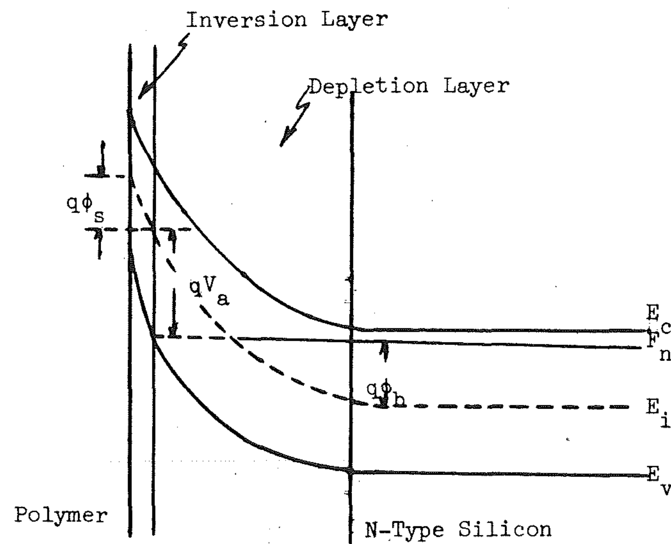

Figure 18

Because of the relatively large conductance of the inversion layer, the entire bias, V_a, appears across the depletion region between the inversion layer and the bulk. Thus, V_a is actually the V_s as defined in Figure 14b.

Therefore, the generation current can be expressed as

$$I_{gen} = 1/2 \; q \; \frac{Ni}{\tau_o} \left\{ \frac{2K_s\varepsilon_o}{qN_d} \quad (\phi_b + \phi_s + \; Vs) \right\}^{1/2} Aj$$

it will increase with square root voltage drop across semiconductor. The increase is very small, any increase in polymer voltage is exceedingly small.

Current in region (3) of the MPS device is limited by the diffusion and generation currents in the field-induced p-n junction. The diffusion current component is independent of bias voltage, however, and the limiting term is actually the electron-hole pair generation in the depletion region.

An important point is that the generation current is dependent upon the width of depletion layer. For higher resistivity semiconductors the doping density is lower, thus the width is larger and a higher saturation current level should be observed for the MPS devices. On the other hand, for MPS devices made on lower resistivity semiconductors it is expected the current would be saturated at lower level. This is exactly what our experimental data show. Referring to figures 11 and 12, it can be seen the device (#81) of lower resistivity (70Ω cm) saturated at a level lower than the higher resistivity devices (#54 and 55, 113Ω cm).

Besides the generation and diffusion currents, leakage and avalanche effects may exist in the MPS device system. When one or both of them exists the reverse current may never become saturated, or may saturate at higher level.

A cross-section area picture for a MPS device of reverse bias is shown below

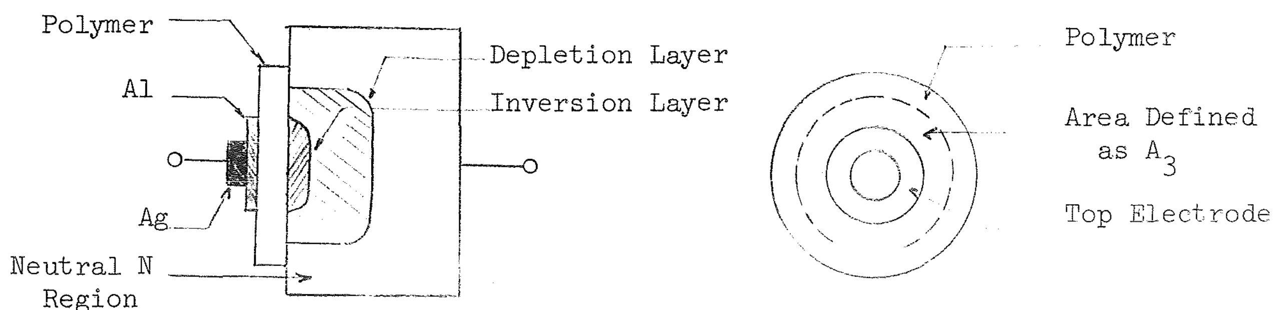

Figure 19 Cross Section of an MPS Device

The surface states at the interface of the polymer and semiconductor may act as traps or recombination centers. Thus, it may contribute a surface component of current by releasing carriers from traps. This can be expressed as

$$I_s = q\, U_s A_s$$

where A_s is the area defined in Figure 19, and

U_s is the carrier generation rate per unit surface area and is a function of surface state density, their capture cross section and thermal velocity of carriers.

Those surface states may serve as a by-pass between the inversion layer and the N-type neutral region. Thus the MPS device may not saturate as it should. This also explains why the current through MPS devices in reverse-biased condition is extremely sensitive to surface preparation.

Within the field-induced junction, defects may be present. Those defects will lower the breakdown voltage of the field-induced junction, thus a large excess reverse current will be observed even at relatively low reverse biases. Current saturation can never be seen in this case. Defects may be introduced by mechanically lapping and polishing the silicon wafers. Strong chemical etching may eat away the defects and yield better results. This serves to explain why adequate chemical etching is preferred for observation of current saturation of MPS devices.

CHAPTER V

CONCLUSION

The electrical conductivity of thin polymer films produced by electron bombardment of D.C. 704 diffusion pump oil does not appear to be explained completely by any one of the simple mechanisms theoretically applicable to thin dielectric films. The observed behavior can be described satisfactory by Poole-Frenkel emission at room temperature. Even then the description is not completely adequate, because the I-V Characteristic may have two or more asymptotes. A combination of Poole-Frenkel and Schottky emissions may have to be assumed to justify the slope changes. For example two types of defects with Poole-Frenkel behavior may adequately characterize charge transport through the polymer.

The limiting electron-hole pair generation in the depletion region after the MPS device has been strongly inverted explains the current saturation of MPS devices in reverse bias condition. This saturation may not be observed because surface leakage current introduced by surface states in the polymer-semiconductor interface. The defects within the field-induced P-N junction may contribute a current component, thus saturation may also not be observed. These also explain why the MPS device is extremely sensitive to surface preparation silicon of higher resistivity and strong chemical etching seems to yield best results.

The purpose of this research project is to build a voltage/ current digital transducer by interconnection several of these saturating

MPS devices. Experimental results showed this is very possible. For obtaining stable and reproducable results, the silicon may have to be protected by an oxide layer. Silicon dioxide would be grown on the silicon surface first, and then window opened by using photo resist technique. The polymer would then be deposited in the windows to make the MPS devices. The MPS devices could then serve as the "stepping stones" to build voltage/current digital transducers and also provides a way of study the semiconductor surface properties.

BIBLIOGRAPHY

1. G. Glocker and S.C. Lind, The Electrochemistry of Gases and Other Dielectrics, J. Wiley and Sons, Inc., New York, 1939.

2. J. Hillier, "On Investigation of Specimen Contamination in Electron Microscope," J. Appl. Phys., Vol. 19, No. 3, Mar., 1948, pp. 226-30.

3. J.H.L. Watson, "Effect of Electron Bombardment Upon Carbon Black," J. Appl. Phys., Vol. 18, No. 2, Feb., 1947, pp. 153-61.

4. L. Holland and L. Laurenson, "The Electrical Properties of Silicone Films Polymerized by Electron Bombardment," Vacuum, Vol. 14, June, 1964, pp. 325-332.

5. D.R. Lamb, Electrical Conduction Mechanisms in Thin Insulating Films, Spottiswoode, Ballantyne and Co., Ltd., London, 1967.

6. J. Frenkel, "Pre-Breakdown Phenomena in Insulators and Electronic Semiconductors," Phys. Rev., Vol. 54, 1938, pp. 647.

7. L.L. Chang, P.J. Stiles, and L. Esaki, "Electron Tunneling Between a Metal and a Semiconductor: Characteristics of Al-Al_2O_3-SnTe and - GeTe Junctions," J. Appl. Phys., Vol. 38, No. 11, Oct., 1967, pp. 4440-4445.

8. W.E. Dahlke, "Tunneling into Interface States of MOS Structures," App. Phys. Letters, Vol. 10, No. 10, May, 1967, pp. 261-262.

9. C.W. Wilmsen, "Tunneling Between a Metal and Silicon Separated by a Polymer Insulator," Dissertation, University of Texas, 1967.

10. L.V. Gregor and L.H. Kaplan, "Electrical Conductivity of Thin Polymer Films," Thin Solid Films, Vol. 2, Jan., 1968, pp. 95-103.

11. E.T. Fitzgibbons, "Charge Transport Mechanisms in Thin Polymer Films," Thesis, University of Texas, 1967.

12. P.R. Emtage and W. Tantraporn, "Schottky Emission Through Thin Insulating Films," Phys. Rev. Letters, Vol. 8, No. 7, Apr. 1, 1962, pp. 267-268.

13. J.T. Wallmark and H. Johnson, Field-Effect Transistors, Prentice-Hall, Inc., Englewood Cliffs, New Jersey, 1966.

14. J.L. Moll, Physics of Semiconductors, McGraw-Hill, New York, 1964.

15. R. Stratton, "Volt-Current Characteristics for Tunneling Through Insulating Films, J. Phys. Chem. Solids, Vol. 23, 1963, pp. 1177-1190.

16. J.G. Simmons, "Potential Barriers and Emission-Limited Current Flow Between Closely Spaced Parallel Metal Electrodes," J. Appl. Phys., Vol. 35, No. 8, Aug, 1964, pp. 2472-2481.

17. J.W. Conley, C.B. Duke, G.D. Mahan, and J.J. Tiemann, "Electron Tunneling in Metal-Semiconductor Barriers," Phys. Rev., Vol. 150, No. 2, Oct. 1966, pp. 466-469.

18. P.V. Gray, "Tunneling from Metal to Semiconductors," Phys. Rev., Vol. 140, No. 1A, Oct., 1965, pp. A169-A186.

19. J.G. Simmons, "Generalized Formula for the Electric Tunnel Effect Between Similar Electrodes Separated by a Thin Insulating Film," J. Appl. Phys., Vol. 34, No. 6, June, 1963, pp. 1793 -1803.

20. J.R. Yeargan, "Charge Transport Mechanisms in Thin Silicon Nitride Films," Dissertation, University of Texas, 1967.

21. J.G. Simmons, "Poole-Frenkel Effect and Schottky Effect in Metal-Insulator-Metal Systems," Phys. Rev., Vol. 155, No. 3, Mar., 1967, pp. 657-660.

22. J.G. Simmons,"Transition from Electrode-Limited to Bulk-Limited Conduction Processes in Metal-Insulator-Metal Systems," Phys. Rev., Vol. 166, No. 3, Feb., 1968, pp. 912-920.

23. A. Many, Y. Goldstein, and N.B. Grover, Semiconductor Surfaces, John Wiley and Sons, Inc., New York, 1965.

24. R.M. Warner, Integrated Circuits Design Principles and Fabrication, McGraw-Hill Co., New York, 1965.

25. D.R. Frankl, Electrical Properties of Semiconductor Surfaces, Pergamon Press, Ltd., Oxford, 1967.

26. N.F. Mott and R.W. Gurney, Electronic Processes in Ionic Crystals, Dover Publications, Inc., New York, 1964.

27. F.J. Biondi, Transistor Technology, Vol. III, Bell Lab Series, Nostrand Co., Inc., Princeton, New Jersey, 1958.

28. A.E. Ennes, "Sources of Electron-Inducted Contamination, in Kinetic Vacuum Systems," Brit. J. Appl. Phys., Vol. 5, No. 1, 1954, pp. 27-31.

29. R.W. Christy, "Formation of Thin Polymer Films by Electron Bombardment," J. Appl. Phys., Vol. 31, No. 9, Sept., 1960, pp. 1680-3.

30. R.N. Hall, "Electron-Hole Recombination in Germanium," Phys. Rev., Vol. 87, 1952, P. 387.

31. W. Shockley and W.T. Read, "Statistics of the Recombination of Holes and Electrons," Phys. Rev., Vol. 87, 1952, pp. 835-844.